Earth's Future

RESEARCH ARTICLE
10.1029/2023EF004117

Special Collection:
CMIP6: Trends, Interactions, Evaluation, and Impacts

Storylines for Global Hydrologic Drought Within CMIP6

N. Bjarke[1], B. Livneh[1,2], and J. Barsugli[2,3]

[1]Department of Civil, Environmental, and Architectural Engineering, University of Colorado, Boulder, Boulder, CO, USA, [2]Cooperative Institute for Research in Environmental Sciences (CIRES), Boulder, CO, USA, [3]National Atmospheric and Oceanic Administration – Physical Sciences Laboratory, Boulder, CO, USA

Abstract Future global increases in the duration and severity of hydrologic drought present an emerging challenge for water resource management. However, projected changes to drought within global climate models are often complex, including potentially co-occurring changes to the timing, duration, and severity of drought. Here, we apply a storyline approach for interpreting projections of future hydrologic drought to identify coherent narratives that include runoff trends, shifts in the seasonal drought timing, increases in multi-year drought frequency, and increased drought severity within the Coupled Model Intercomparison Project Phase 6. We develop a framework to classify future drought storylines (2015–2100) and quantify model consensus to determine the most-likely "dominant" storyline under four emission scenarios Shared Socioeconomic Pathways (SSPs) 1–2.6, 2–4.5, 3–7.0, and 5–8.5. Under a low-emission scenario (SSPs 1–2.6) approximately one third of the land-area is projected to be impacted by a dominant storyline of minimally detectable runoff trend paired with increased frequency of multi-year drought. However, under the highest-emission scenarios (SSPs 5–8.5), the most likely storyline shifts to an increase in multi-year drought frequency, increased severity of drought, and negative long-term runoff trends for 62% of the area in those same regions. Shifts in the seasonal timing of drought are a component of dominant storylines for the northern latitudes across all emission scenarios. These results provide an alternative mode of interpretation of co-occurring changes to the features of future drought, framed in a way to support regional adaptation strategies to mitigate future drought impacts.

Plain Language Summary Future hydrologic droughts are projected to become more severe and prolonged through the 21st century, posing challenges for water resource management across the globe. To understand these changes, we analyzed and ensemble of global climate models, focusing on runoff trends, shifts in seasonal drought timing, increased multi-year drought frequency, and severity. Using a storyline approach, we identified coherent narratives for future drought scenarios from 2015 to 2100 under different emission scenarios. Under low-emission scenarios, about one-third of the land may experience minimal runoff changes but increased multi-year drought frequency. However, under high-emission scenarios, many global regions are projected to experience widespread multi-year droughts, intensified drought severity, and decreased runoff. Furthermore, seasonal shifts in drought timing were prominent in northern latitudes across all future scenarios. These findings offer insights to support regional adaptation strategies to address future drought impacts.

Key Points:

- Future storylines that include more frequent multi-year drought occur for at least 23% of the land-surface in all future emission scenarios
- Seasonal shifts in the timing of drought occur in the dominant storyline for the northernmost latitudes regardless of emission scenario
- Hydrologic drought storylines that will most acutely stress water resources become more extensive under higher emission scenarios

Supporting Information:

Supporting Information may be found in the online version of this article.

Correspondence to:

N. Bjarke,
Nels.Bjarke@colorado.edu

Citation:

Bjarke, N., Livneh, B., & Barsugli, J. (2024). Storylines for global hydrologic drought within CMIP6. *Earth's Future*, *12*, e2023EF004117. https://doi.org/10.1029/2023EF004117

Received 13 SEP 2023
Accepted 25 APR 2024

1. Introduction

Droughts have become more severe and have increased in duration for many regions across the globe in recent decades, with general circulation models (GCMs) projecting that these trends will continue as global temperatures rise (Cook et al., 2020; Zhao & Dai, 2022). However, investigations into future projections reveal that different features of drought may change simultaneously (Zhao & Dai, 2022), adding complexity to narratives of understanding water scarcity. Previous literature has focused on describing potential future changes to extended surface water deficits by calculating the summary statistics from an ensemble of GCM projections and reporting alterations to each feature of drought, such as duration and severity, independently (Cook et al., 2020; Gessner et al., 2022; Ukkola et al., 2018; T. Wang et al., 2021; Zhao & Dai, 2022). However, reporting summary ensemble statistics may neglect to convey how alterations to drought features co-occur within individual future projections (Leonard et al., 2014; Zscheischler et al., 2018) and which combinations of changes are most likely. To further understanding of simultaneous changes within future projections, this manuscript explores the use of "storylines" as a tool for categorizing multiple co-occurring changes to drought into physically plausible scenarios. We develop these storylines from an ensemble of Coupled Model Intercomparison Project—Phase 6 (CMIP6) GCMs,

identifying the most likely pathways of the severity, duration, frequency, and seasonal timing of drought paired with long-term trends in runoff.

Hydrologic drought can be generally described as a shortage of surface water, but any single drought event is unique in its features and may require a unique adaptation approach (Frederick & Major, 1997; Kundzewicz et al., 2008; Olmstead, 2014). For example, an acute and short-lived drought may be relatively manageable (L. G. Chen et al., 2019; Christian et al., 2019, 2021; Yuan et al., 2019) compared to a less acute but longer duration drought that may push water storage infrastructure past critical thresholds (Cayan et al., 2010; Heim, 2002; King et al., 2020; Nicholls, 2004; Páscoa et al., 2017; Van Dijk et al., 2013; Vicente-Serrano, 2006; Woodhouse et al., 2010). In this way, drought severity—defined here as the magnitude of water shortage over a period of time relative to a historical baseline—may vary in its impacts, dependent on another feature of the drought such as duration—the length of time that a drought persists. Each feature of drought can also vary in its significance for adaptation on different timescales. For example, one could consider changes to the frequency of drought—the expected number of occurrences of drought events within a decade or several decades—to inform long term water resource planning (Carlton et al., 2016; McNeeley et al., 2016; Rajagopalan et al., 2009; Zeff et al., 2016). Alternatively, one could evaluate shifts in the seasonal timing of drought to inform adaptations to water management on an annual timescale. These features of drought and their potential future changes can also be viewed in conjunction with long-term projected trends in runoff to develop effective adaptation strategies for water resources (Anisimov et al., 2007; IPCC, 2021).

Previous analyses of the CMIP6 ScenarioMIP (O'Neill et al., 2016) simulations have shown projected increases in the severity and duration of drought as a response the increase in the atmospheric concertation of greenhouse gases (Cook et al., 2020; H. Li et al., 2021; T. Wang et al., 2021; Zhao & Dai, 2022). Widespread increases in agricultural and hydrologic drought severity occur within CMIP6 simulations across western North America, Europe, the Mediterranean, northern South America, southern Africa, southeast Asia and Australia (Cook et al., 2020). CMIP6 projected increases in severity of drought are shown to be greatest in magnitude across historically arid regions (Cook et al., 2020; H. Li et al., 2021), driven by changes to the long-term balance of precipitation and evaporative demand (H. Li et al., 2021; T. Wang et al., 2021; Zhao & Dai, 2022). Increasing prevalence of drought conditions during the warm season has been attributed to earlier seasonal snowmelt which shifts the timing of runoff generation and extends the snow-free time when surface water can be lost to evapotranspiration (Barnett et al., 2005; Cline, 1997; Cook et al., 2020; Siirila-Woodburn et al., 2021; Zhao & Dai, 2022). The severity and timing of seasonal hydrologic drought has also been shown to coincide with altered precipitation patterns driven by ENSO teleconnections (Anderegg et al., 2015; Campbell et al., 2011; Williams et al., 2015). In addition to increases in severity, duration of both agricultural and hydrologic drought is projected to increase (Cook et al., 2020; Zhao & Dai, 2022), with multi-year droughts becoming more frequent as global temperatures rise (Gessner et al., 2022; T. Wang et al., 2021).

Though these previous analyses provide useful insight into future drought changes, many report summary ensemble statistics to describe changes to single hydrologic features independently. This may overlook key interactions between drought features within individual simulations (Leonard et al., 2014; Zscheischler et al., 2018). Storylines offer an alternative way to understand likely changes to hydroclimate with an emphasis on the plausibility of physical land-surface and atmosphere interactions (Shepherd et al., 2018). Storyline approaches have been used to investigate probable future pathways of changes to the climate such as trends precipitation as they relate to atmospheric circulation patterns (Schmidt & Grise, 2021), the socio-economic impacts of extreme climate events (Goulart et al., 2021; van den Hurk et al., 2023), and the compounding probabilities of extreme events (Ciais et al., 2005; Leonard et al., 2014; Zscheischler et al., 2018). In the context of drought, storyline classification can be a powerful tool for evaluating change, allowing for explicit consideration of interactions between changes to drought features and trends (Gessner et al., 2022). This is critical because extreme events like drought have been shown to covary with other extremes (Chan et al., 2022; Ciais et al., 2005; Leonard et al., 2014; Mazdiyasni & AghaKouchak, 2015; Zscheischler et al., 2018) and depend on unique atmospheric circulation patterns or temporal sequencing of meteorological fluxes (Chan et al., 2022; Gessner et al., 2022; van der Wiel et al., 2021; van Garderen & Mindlin, 2022).

The storyline approach also has the utility of being moldable to directly answer specific questions about hydroclimate change, such as, where will hydrologic drought features change in ways that are most likely to stress water resource systems? In this analysis we use storylines to evaluate three features of drought change that stress

water resources—increasing frequency of multi-year drought, magnification of annual drought severity, and seasonal shifts in drought timing—paired with long-term trends in surface runoff. We seek to understand regional differences in the drought storylines that are most likely to occur and how the spatial distribution of these storylines changes as emissions become more severe through the 21st century. This analysis is unique in that it addresses the need consider concomitant changes to hydrologic drought features and surface water availability (Budescu et al., 2012; Shepherd & Lloyd, 2021), while focusing on identifying the likelihood storylines that could potentially stress water resource systems (Dessai & Hulme, 2004; Herrando-Pérez et al., 2019).

2. Data and Methods

This section describes the data used and methodologies applied in the evaluation of the dominant projected storylines of hydrologic drought change across an ensemble of CMIP6 simulations. The first subsection contains a description of the classification of storylines (Section 2.1). Following that are descriptions of the methods for drought quantification using the Streamflow Drought Index (SDI) (Section 2.2), evaluation of statistically significant trends in runoff and SDI intensity (Section 2.3), quantification of changes to the frequency of droughts lasting multiple years (Section 2.4), and detection of seasonal shifts in the timing of drought (Section 2.5). The last subsection includes a list of GCM projections that are used within this analysis (Section 2.6) along with a description of models, emission scenarios, and model output variables used for drought quantification.

2.1. Classification of Dominant Drought Storylines

We propose a method to classify hydrologic drought storylines by combining projected changes in drought features (Sections 2.3–2.5) with long-term runoff trends (Section 2.3). For each grid cell in a model simulation, storylines are classified based on runoff trend and three potential changes to drought features: (a) increase in annual drought severity (positive annual SDI trend), (b) increase in multi-year drought frequency, and (c) seasonal shifts in the drought timing resulting in increased drought frequency in the cold or warm season (Figure 1). Storylines are classified based on the direction of drought feature changes rather than magnitude to reduce the influence of the biases of simulated hydrologic fluxes within GCMs (H. Chen & Xu, 2020; Dong et al., 2020; Lehner et al., 2019). The method of reporting directional change has been suggested as a way effectively support the needs of water policy decision making (Barsugli et al., 2012; Brown et al., 2019).

The pairing of runoff trends with changes in drought features yields nine potential storylines (Figure 1). We count the number of models that agree on each storyline category for the future projected period for a single common grid cell and for each future emission scenario. A single model run is used for each GCM. We classify the dominant storyline as the one that the greatest number of models produce in the future period and require that a simple majority of GCMs reach consensus on the dominant storyline across the ensemble. Only five out of the nine possible storylines tested here are classified as dominant storylines (those shown in Figure 1), meeting the minimum criteria of majority model consensus for at least 0.1% of land area grid cells. The remaining storylines that are not included in Figure 1 do not occur in any of the CMIP6-MME simulations or occur in less than 0.1% of the land area.

Counting models is an effective method to characterize projected changes across GCMs (Tebaldi et al., 2011) as used here to highlight areas of statistically significant agreement in future change. Considering that the structural similarities among GCMs within the CMIP ensembles might influence the dominance of any single storyline (Knutti et al., 2013), we assess the sensitivity of the classification of each dominant storyline using a bootstrap resampling approach. For each emission scenario 500 random sub-samples of half ($n = 12$) of the GCMs are selected. The dominant storylines are determined at each grid cell for each of the 500 sub-samples. Dominant storyline uncertainty is estimated by calculating the percentage of the land area projected to experience each storyline across the resampled iterations.

While the focus is on the dominant storyline as the most likely pathway for hydrologic drought, secondary storylines are also considered because storylines are not mutually exclusive (more than one storyline may occur in more than half the models). For example, if a location has 15 out of 24 models simulating Storyline 1 (S1) and 13 models simulating Storyline 2 (S2), S1 is conserved dominant and S2 secondary. Figure 7 reports locations where secondary storylines emerge with less model agreement than the dominant storyline, but still meeting the minimum threshold for model agreement.

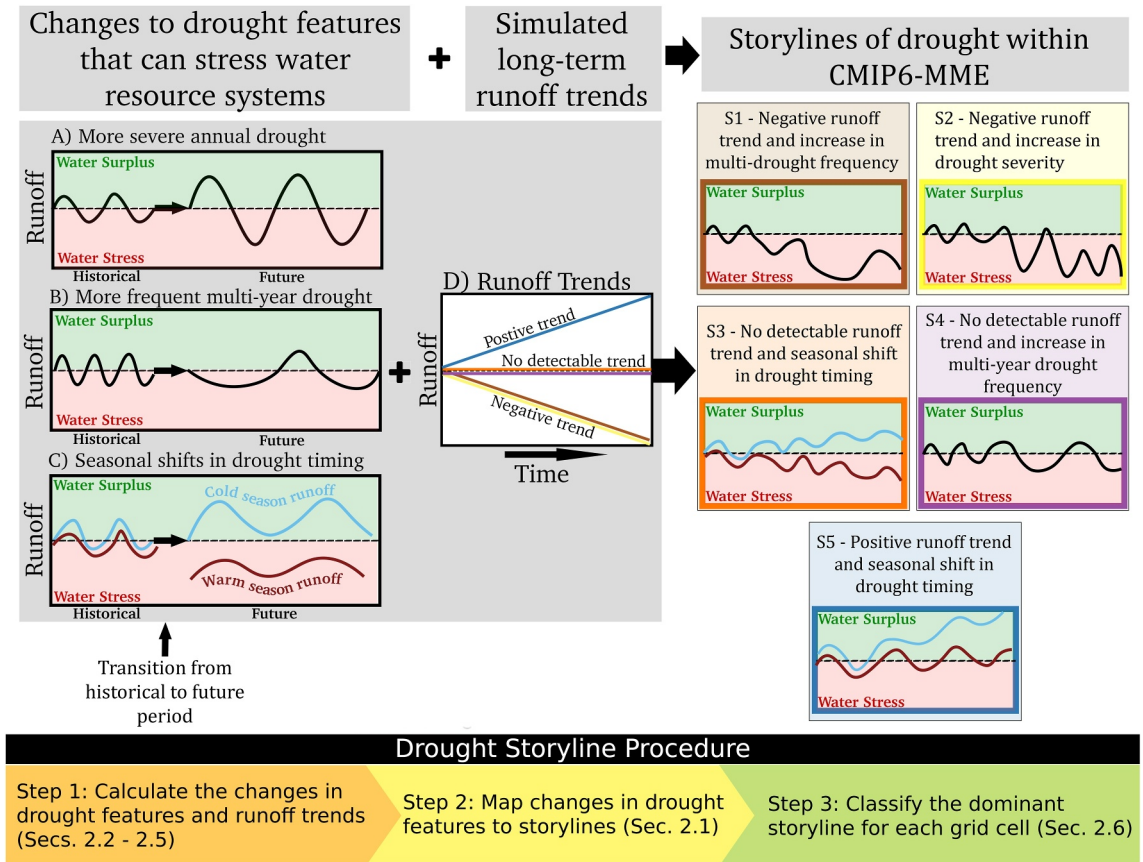

Figure 1. Schematic of hydrologic drought storyline generation and storylines present within the CMIP6-MME. Panels (a–c) show conceptual changes to hydrologic drought features from a historical to future period, the first component of each storyline. The dashed line represents average runoff conditions, where "water surplus" periods are above and "water stress" periods are below the line. Panel (a) demonstrates an increase in the severity of future droughts, panel (b) demonstrates a shift to more frequent multi-year droughts, and panel (c) demonstrates seasonal shifts in drought timing. Panel (d) provides the potential pathways for runoff trends in the CMIP6 general circulation model (GCM) simulations (the second component of each storyline), with a colored line corresponding to one of five dominant storylines. All the storylines shown (colored panels on the right side of the figure) are dominant storylines of future drought that occur within the CMIP6 projections. Within these panels, we schematically demonstrate how the frequency, duration, and timing of periods of water stress or surplus change in locations where each of these storylines are dominant. A simple flowchart is provided at the bottom of the figure to describe how the dominant storyline is classified for each grid cell across the ensemble of CMIP6 GCMs.

2.2. Streamflow Drought Index (SDI)

The frequency and severity of drought are quantified with the SDI (Nalbantis & Tsakiris, 2009) given its past utility in evaluating hydrologic drought across an ensemble of GCMs (T. Wang et al., 2021; Zhao & Dai, 2022). SDI has utility, as applied here, because it considers normalized deviations from climatological runoff for each GCM relative to the historical simulation. Normalization is important for combining hydrologic drought projections across GCMs in a way that minimizes the impact of runoff biases from each model. Other commonly used drought indices are potentially less desirable than SDI for the purpose of evaluating surface water availability. For example, the Standardized Precipitation Index only considers the amount of precipitation and does not explicitly consider losses to evaporation or subsurface abstractions. The Standardized Precipitation-Evapotranspiration Index does include an estimation of the balance between incoming precipitation and the evaporative loss, but offline estimations of potential evapotranspiration are required (Bjarke et al., 2023) and do not directly reflect the balance of precipitation and actual evapotranspiration on a monthly timescale (Jiang et al., 2023; Van der Schrier et al., 2011).

To compute SDI (Equations 1 and 2), we follow the guidance of Nalbantis and Tsakiris (2009), quantifying drought periods of varying length (6-, 12-, and 24-month) to evaluate changes in seasonal, annual, and multi-annual modes of drought. To quantify seasonal changes, we use a 6-month aggregation period to account for shifts in drought occurrence from the warm to cold season (or cold to warm season) (Cook et al., 2020), while

avoiding shorter seasonal classifications that could be more strongly affected by model biases in the timing of runoff generation (H. Li et al., 2021). It is possible that shorter seasonal shifts could occur within the GCMs. The 12-month period was chosen to quantify the severity of annual drought. The 24-month period is used to evaluate the occurrence of multi-year drought, drought conditions that persist for longer than a single annual period. It is possible to use a longer aggregation period for multi-year droughts, but in the interest of using storylines to communicate clear future climate pathways, we are simply reporting changes to the probability of droughts lasting two years, but these could potentially be part of an even longer drought event beyond 24-month.

In our quantification of SDI we use:

$$V_{i,k} = \sum_{j=1}^{3k} Q_{i,j} \; ; \; i = 1,2, ..., n, j = 1, 2, \ldots, 12, k = 2,4,8 \tag{1}$$

where $V_{i,k}$ is the cumulative, log-transformed streamflow for the ith water year, jth starting month, and kth 3-month accumulation periods. For example, when k is equal to four, we are evaluating the 12-month drought accumulation. We log-transform the accumulated streamflow for each V-value following Nalbantis and Tsakiris (2009) to reduce the impact that skew can have on the normalization of hydrologic data and the associated quantification of probability of drought (McKee et al., 1993). This results in time series of V-values for each grid cell that can then be used to quantify the deficit of runoff flow relative to the period of accumulation of interest, here we use k-values of 2, 4, and 8 which represent 6, 12, and 24 months respectively. SDI is then calculated from the series of V-values using the following equation:

$$\mathrm{SDI}_{i,k} = \frac{V_{i,k} - \overline{V}}{s_k}; i = 1, 2, \ldots, n, k = 2,4,8 \tag{2}$$

Where $\overline{V}$ and s_k are the mean of the log-transformed accumulated runoff from the series of V-values for the k reference period from the historical simulation and the standard deviation of those values. $V_{i,k}$ is the series of log-transformed accumulated runoff for 6, 12, and 24 months periods.

2.3. Trends in Runoff and SDI

We assess projected trends in total water-year surface runoff (aggregated from 1 October to 30 September the following year) for each grid cell in each of the CMIP6-MME simulations. Using ordinary least squares regression, we analyze annual runoff values from 2015 to 2100 for statistical significance with a two-sided Wald Test (Wackerly et al., 2104) to detect simple linear trends. All runoff trends are assessed with a 90th percentile confidence interval (5% confidence in either positive or negative trend respectively), classifying each grid cell categorically as having a positive, negative, or undetectable trend. The 90th percentile threshold is chosen to ensure consistency with the confidence interval of tests applied to the one-sided projected changes to drought features described below.

Consistent methodology is applied to calculate trends in annual SDI. SDI is calculated annually ($k = 4$ in Equations 1 and 2) with October as the initial month, and a simple linear regression is performed to determine long-term (2015–2100) trends. October is chosen as the starting month to align with the low runoff period of the annual hydrologic cycle of the northern hemisphere, consistent with the span of the water-year. To confirm that this choice did not significantly bias the results, particularly for the southern hemisphere, the analysis was repeated using January, April, and July as starting month as well with no qualitative difference in the spatial distribution of dominant storylines. Trends in SDI are assessed for statistical significance above a 95th percentile threshold using a one-sided Wald Test with a t-distribution (Wackerly et al., 2014), allowing for consistency with the significance of potential positive runoff trends described above. Grid cells with positive trends indicate projected increases in annual drought severity through the 21st century.

2.4. Multi-Year Drought Frequency

We classify multi-year drought by calculating the SDI over a 24-month (Equations 1 and 2). A multi-year drought is identified if $\mathrm{SDI}_{k=8}$ is less than or equal to −1.0, indicating a moderate drought as classified by Nalbantis and

Tsakiris (2009). This classification begins at the start of the water year (October 1st), where a 24-month period with SDI less than or equal to −1.0 is considered a drought event compared to the historical baseline. We quantify the frequency of multi-year moderate drought events in the historical simulation (1950–2014) for each GCM as percent of the total period spent in multi-year drought and then calculate the percent change in the frequency of multi-year drought within the future projected period (2015–2100). The increases in multi-year drought frequency shown are an indication of an increase in the probability of historical 24-month hydrologic drought levels within the future projected period for each GCM in the CMIP6-MME under all four emission scenarios. All increases in the frequency of multi-year drought occurrence of less than 5% from the historical to future periods are considered insignificant.

2.5. Seasonal Droughts

The estimate of seasonal changes in the frequency of drought is designed to evaluate whether temporal shifts in the timing of runoff generation are causing seasonal shortages in total runoff. Following the seasonal subdivisions used in Cook et al. (2020) and Zhao and Dai (2022), we evaluate shifts in hydrologic drought between two seasons: warm (April–September) and cold (October–March) seasons in the northern hemisphere. This is primarily motivated to capture the timing of snowmelt and changes in phase of precipitation from snow to rain (Barnhart et al., 2020; Cohen et al., 2015; Neelin et al., 2013; Whitfield & Shook, 2020) that could alter the amount of surface water generated, particularly in snow-dominated regions. We determine a seasonal shift to have occurred if either the frequency of warm season droughts has increased and the frequency of cold season droughts has decreased, or vice versa. We describe in detail the direction of the shift in the discussion.

We express seasonal shifts as percent change in the probability that drought will occur in one season relative to the other (as described in Equation 3):

$$\text{Seasonal Shift} = (P(\text{SDI}_{\text{Warm,Future}} < -1.0) - P(\text{SDI}_{\text{Warm,Historical}} < -1.0)) - (P(\text{SDI}_{\text{Cold,Future}} < -1.0) - P(\text{SDI}_{\text{Cold,Historical}} < -1.0)) \quad (3)$$

Where $P(\text{SDI}_{X,Y})$ is the empirical probability of a 6-month drought (SDI < −1.0) occurring for the X-season (warm or cold defined in reference to the Northern Hemisphere) within the Y-period (historical or future simulation within each GCM). The change in that probability between the two seasons from the historical and future period are calculated to determine seasonal shifts for all emission scenarios. For example, if a GCM produces a 10% decline in the probability of drought during the cold season and 20% increase in the probability of drought during the warm season, then we report this as a 30% shift in the probability. We only report seasonal shifts using a minimum threshold of a ±5% change in probability. To indicate the direction of the seasonal drought probability shift, we use positive values to indicate where there is an increase in the probability of northern hemisphere warm season (April—September) hydrologic drought (and decline in the probability of northern hemisphere cold season drought). Negative values indicate an opposite direction of the probability change. Similar to our approach in evaluating trends in the water-year SDI and runoff (Section 2.3), we tested alternative starting dates for the 6-month seasons and found that the maximum frequency of seasonal shifts occurs from the northern hemisphere warm to cold season or vice versa.

2.6. CMIP6 Multi-Model Ensemble (CMIP6-MME)

We select a multi-model ensemble of 24 CMIP6 GCMs based on the availability of (a) the total runoff output variable (mrro) at the monthly temporal resolution, (b) simulations of the "historical" period from the CMIP6 DECK experiments (Eyring et al., 2016), (c) simulations forced using the four future Shared Socioeconomic Pathways (SSP) emission scenarios, and (d) full and complete data records from 1950 to 2014 for the historical simulation and 2015–2100 for all future SSP simulations on the CMIP6 database (https://esgf-node.llnl.gov/projects/esgf-llnl/). These year ranges are used because they are the years available across all model simulations described below for the historical and future periods respectively. All GCMs that fit these criteria at the time of data acquisition were downloaded and are described below.

Suitability of the CMIP6-MME for drought storylines: Estimation of future hydrologic drought change using simulated runoff from GCMs can raise concerns due to previously observed limitations in simulated hydrology.

Previous studies have noted potential issues in GCM hydrology including: simulated precipitation biases (H. Chen & Xu, 2020; Coats et al., 2013; Srivastava et al., 2020; B. Zhang & Soden, 2019), significant variability in simulated runoff responses to changes in the water-energy balance (Lehner et al., 2019; Zhou et al., 2019), and poorly constrained observational baselines to validate drought within models (Lian et al., 2018; Orlowsky & Seneviratne, 2013; Padrón et al., 2019; Ukkola et al., 2018). Stated alternatively, short and spatially disparate observational records of streamflow can contribute to uncertainties in the validation of GCM simulations of drought (Padrón et al., 2019; Ukkola et al., 2018).

Despite these known limitations, previous studies have evaluated the fidelity of simulated runoff within the ensemble of GCMs from CMIP6 and found improvements from previous generations of climate models in terms of both bias and spread of ensemble simulated hydrology (J. Li et al., 2021; A. Wang et al., 2022). The ensemble of GCMs also simulate the seasonal cycle of runoff production and timing of maximum runoff reasonably well for most of the land surface, with median peak timing of runoff across an ensemble of GCMs occurring within 1–2 months of observational data sets (J. Li et al., 2021). Furthermore, numerous studies, as described in Cook et al. (2020), have noted regional consistencies between observational and GCM simulated patterns of drought in recent decades (Garreaud et al., 2020; Hoerling et al., 2012; Otto et al., 2018; Seager et al., 2019). This observational consistency is further demonstrated by the strong correlation of hydrologic drought with drying soil moisture (Hoell et al., 2019; McCabe et al., 2017; Williams et al., 2015) and declining snowpack (Berg & Hall, 2017; Mote et al., 2018) in both observations and simulations as global temperatures rise (Marvel et al., 2019). The simulation fidelity of producing observed drought drivers, our use of a drought metric that normalizes variations of drought to be less sensitive to runoff magnitude biases (Nalbantis & Tsakiris, 2009) and existing validations of drought simulation accuracy within CMIP6 (A. Wang et al., 2022) support that the simulations and methodology applied here are fit for the purpose of determining the dominate storylines of projected drought.

2.6.1. Ensemble of GCMs

We evaluate the dominant hydrologic drought storylines from an ensemble of 24 GCMs (Table S1 in Supporting Information S1), using a single model simulation from each of the GCMs. The native resolutions of the GCMs (described in Table S1 in Supporting Information S1) vary from ∼100 to 250 km, so we re-grid the model output to a common 1° × 1° grid using a conservative remapping algorithm following Zhao and Dai (2015) in order to evaluate the dominant storylines across the ensemble. The re-gridding procedure can impact the bias of climate variables at the daily to sub-daily temporal resolution, particularly within the higher quantiles of the distribution (Rajulapati et al., 2021), but re-gridding GCM output to one resolution for comparison across simulations is common practice when evaluating drought at the monthly time scale (Cook et al., 2020; Papalexiou et al., 2021; Ukkola et al., 2020).

We evaluate the drought storylines within ensembles of four future SSPs: SSP 1–2.6, SSP 2–4.5, SSP 3–7.0, and SSP 5–8.5. These four SSPs represent a range of potential future emission and adaptation scenarios through the 21st century with SSP 1–2.6 (2.6 Wm^{-2} radiative forcing by the year 2100) as the lowest net emission scenario and SSP 5–8.5 (8.5 Wm-2 radiative forcing by the year 2100) as the highest net emission scenario. The first number of the SSP indicates a future projected pathway of socio-economic development and mitigation steps from the global economies that would lead to the a set amount of carbon emissions (O'Neill et al., 2016). The second number of the SSP indicates the increase in net surface radiation in Wm^{-2} and relates each of the pathways to the previous generation, CMIP5, of climate models (O'Neill et al., 2016). All GCMs in the CMIP6-MME are evaluated across the four emission scenarios, with the exception of the HadGEM-GC31-LL model which was not run for the SSP 3–7.0 scenario. For brevity the results shown in the main body of the manuscript, Figures 2–5 only demonstrate the results for a moderate, SSP 2–4.5, and the highest emission scenario, SSP 5–8.5.

3. Results and Discussion

We first show the CMIP6-MME ensemble mean trend in runoff (Figure 2), SDI (Figure 3), changes to multi-year drought frequency (Figure 4) and shifts in the seasonal timing of drought (Figure 5) for comparison to the dominant drought storylines. The ensemble mean is not directly used in each of the storylines, but we show them here to demonstrate how the features of drought change on average across all the GCMs for a low-moderate emission scenario (SSP 2–4.5) and a high emission scenario (SSP 5–8.5). Here we describe regional changes

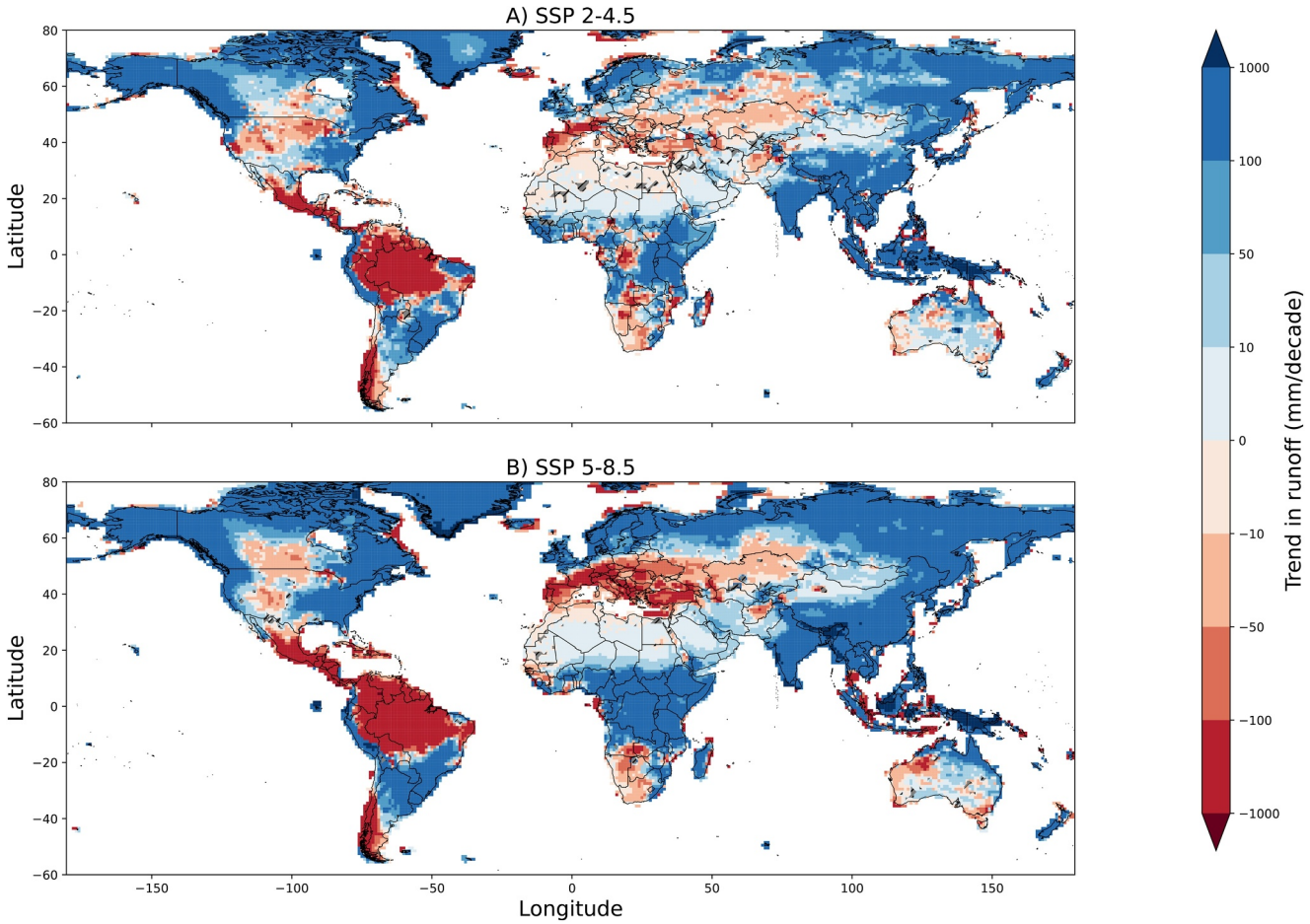

Figure 2. Historical and projected trends in total annual runoff from CMIP6-MME. Ensemble mean trend in annual total runoff estimated for the future projected period for two emission scenarios: Shared Socioeconomic Pathway (SSP) 2–4.5 in the top panel and SSP 5–8.5 in the bottom panel. Ensemble mean total runoff per grid cell (in m/year) are calculated as the mean slope of change in runoff through the future projection period (2015–2100) across the CMIP6-MME. Red shades indicate a decrease in the total runoff and blue shades indicate an increase in the total runoff. Grid cells where fewer than a majority of the models simulate a trend in total runoff with the same sign as the ensemble mean are colored gray and have cross-hatching.

to the ensemble mean within the CMIP6-MME and then highlight where storylines provide additional insight into co-occurring drought changes and model agreement.

3.1. Summary of Individual Components of Drought Storylines Across the CMIP6-MME

Ensemble-mean runoff declines occur in greatest magnitude across central-west North America, the tropical region extending from Central America to northern South America, the southern tips of both South America and Africa, across much of the Mediterranean and central Europe, and along the coastal regions of Australia (Figure 2). The magnitude of the negative ensemble-mean runoff trend increases with the increase in global emissions as shown by differences between SSP 2–4.5 and SSP 5–8.5. This increase in magnitude is most apparent in the tropical region of Central to northern South America. Central Europe and the Australian coastal region both see significant expansions in the area that is impacted by negative runoff trends through the 21st century as a function of the severity of the emission scenario. The spatial pattern of increase in drought severity through the 21st century (Figure 3) is generally consistent with decreases in runoff. However, comparisons of trends in runoff versus trends in SDI do not perfectly spatially correlate, indicating that, even across the model mean, drought severity can change independent of runoff trends. It is difficult to interpret how trends in runoff and the change in SDI co-occur within individual simulations when simply comparing the summary statistics of each change individually.

10.1029/2023EF004117

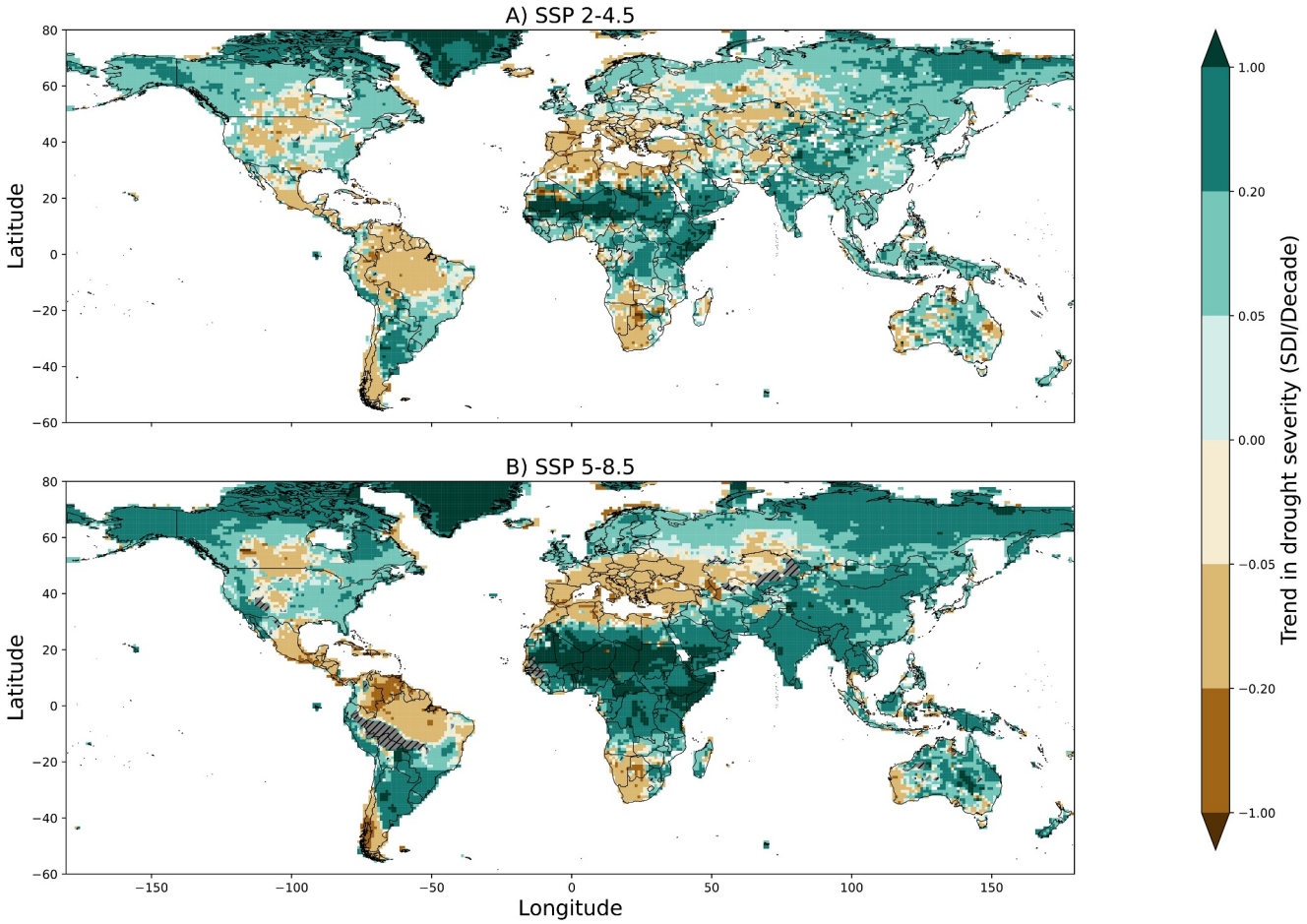

Figure 3. Historical and projected trends in annual Streamflow Drought Index (SDI) calculated from the CMIP6-MME. Ensemble mean trend in annual SDI estimated for the future projected period for two emission scenarios: Shared Socioeconomic Pathway (SSP) 2–4.5 in the top panel and SSP 5–8.5 in the bottom panel. Ensemble mean annual SDI per grid cell (in SDI/year) are calculated as the mean slope annual SDI values through the future projection period (2015–2100) across the CMIP6-MME. Brown shades indicate a decrease in the annual SDI (increase in drought severity) and blue-green shades indicate an increase in the annual SDI (decrease in drought severity). Grid cells where fewer than a majority of the models simulate a statistically significant trend in annual SDI with the same sign as the ensemble mean are colored gray and have cross-hatching.

Changes in frequency are reported as a percent increase in occurrence of multi-year drought per decade (Figure 4). The area of regions impacted by increases in the frequency of multi-year drought, while similarly located to those impacted by declines in total surface runoff (Figure 2), are much more expansive across the land-surface (Figure 4). Changes to the frequency of multi-drought are not strictly driven by declines in runoff since changes to the annual to decadal variability of runoff production can lead to more frequent multi-year droughts. Multi-year drought frequency increases coincide with increase agricultural drought frequency and changes to the balance of precipitation and evaporative demand previously document in CMIP6 simulations (Cook et al., 2020; Zhao & Dai, 2022). Furthermore, comparisons of the ensemble mean changes to the features of drought and ensemble mean trends do not demonstrate how such changes co-vary within each individual GCM simulation. Increases in the frequency of multi-year drought occur for nearly a majority of the land-surface in central North America, Central America, northern and southern South America, Central Europe, the Mediterranean, southern Africa, and south–eastern coastal Australia within both low and high emission scenarios (Figure 4). The magnitude of the increases in multi-year drought are amplified with the global emission scenario, particularly in Central America, northern South America, and the Mediterranean with mean frequency increases in the 21st as great as 30%–50% under SSP 5–8.5 (Figure 4).

Ensemble mean values of hydrologic shifts are the least consistent change, with most of the statistically significant seasonal changes in drought frequency occurring the higher latitudes (>40°N; Figure 5). The spatial

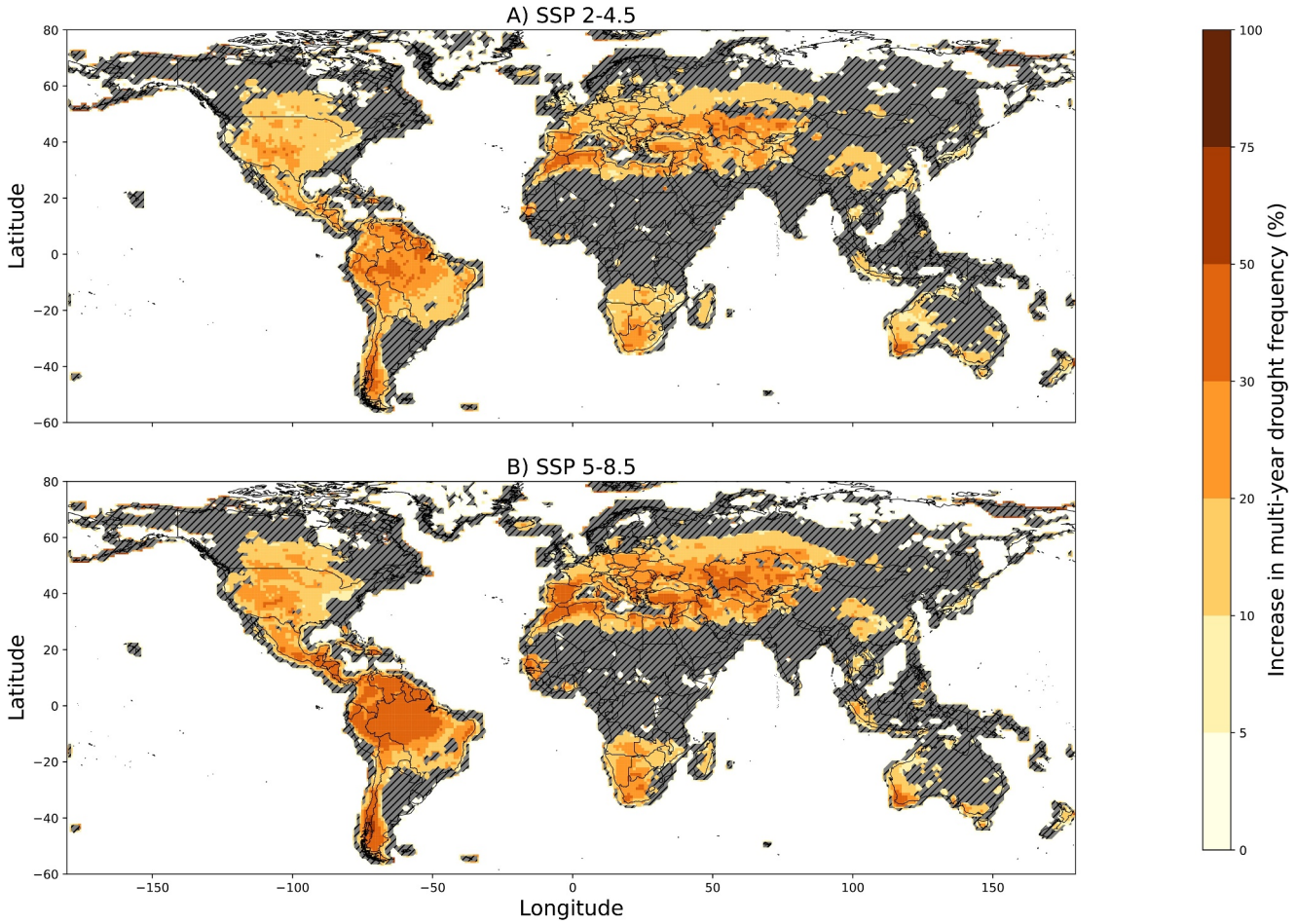

Figure 4. Projected mean increase in the frequency of multi-year hydrologic drought within the CMIP6-MME. Ensemble mean percent increase in the frequency of multi-year drought (Streamflow Drought Index with $k = 8$ in Equation 2) for the future projected period compared to the historical simulation for each general circulation model (GCM) respectively. The top panel is the ensemble mean change within emission scenario Shared Socioeconomic Pathway (SSP) 2–4.5 and the bottom panel is the ensemble mean change within emission scenario SSP 5–8.5. Grid cells where less than a majority of GCMs produce an increase in the frequency of multi-year drought are shaded gray with cross-hatching. Projected ensemble mean changes to the frequency of multi-year drought shown are calculated by taking the mean of the projected multi-year drought frequency increase relative to the historical simulation from each individual GCM. To elaborate on how to read this figure, if a grid cell had a historical average of 1 multi-year drought per decade and experienced a 10% increase in the frequency of multi-year drought per decade in the future projected period, then that grid cell would experience an average of 1.1 multi-year drought per decade.

variability of seasonal shifts is likely due to the timing of snow melt in higher latitudes, as well as overall differences in the precise timing of the wet/dry seasons between the different GCMs in the ensemble causing spatial heterogeneity in the value and significance of the seasonal shifts. The spatial discontinuities in the seasonal shifts and the large fraction of the land-surface that has no significant change in the seasonal shift demonstrates a potential weakness in the approach of using summary statistics based on the ensemble mean.

The northern latitude changes in drought seasonal frequency are spatially consistent with other studies that demonstrate early onset of snowmelt and transition in the phase of precipitation from rain to snow in a warmer future. These changes in the phase of the surface water lead to less runoff production during the warm season and enhanced runoff generation in the cold season, producing more frequent warm season droughts. Seasonal shifts also occur across central and southeast Asia (Figure 5), which is likely driven by changes to the seasonal monsoon cycle observed within CMIP6 (Katzenberger et al., 2021; Park et al., 2020).

The collection of changes in Figures 2–5 are reinterpreted collectively using storylines. The five dominant storylines (Figure 6) are each present within the CMIP6-MME, exhibiting coherent regions within majority model agreement of the simulated trend in runoff and the alteration to hydrologic drought features across the

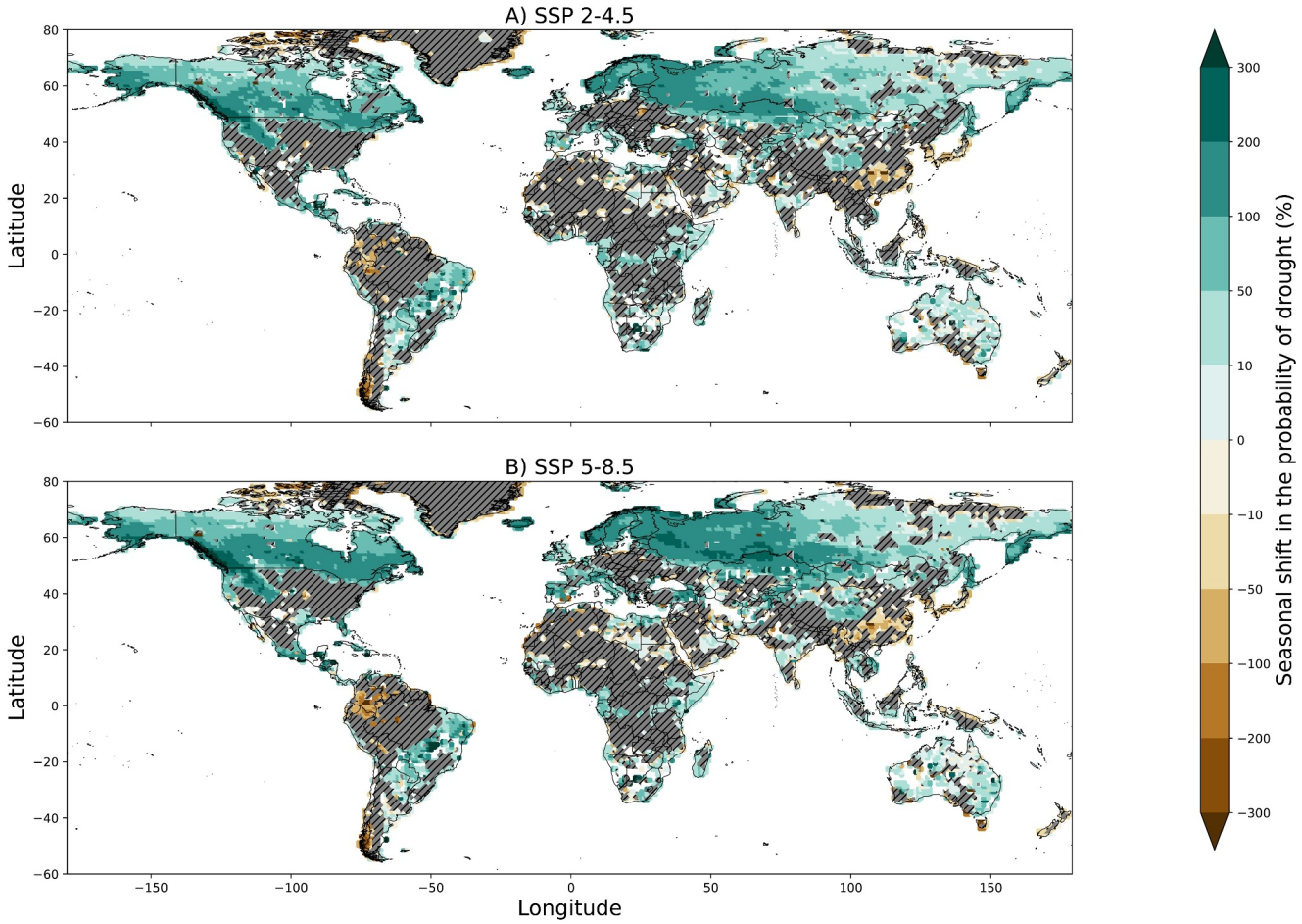

Figure 5. Future projected seasonal shift in the probability of hydrologic drought within the CMIP6-MME. Ensemble mean percent increase in the shift of seasonal drought from warm to cold season or vice versa (Streamflow Drought Index with $k = 2$ in Equation 2) for the future projected period compared to the historical simulation for each general circulation model (GCM) respectively. The top panel is the ensemble mean change in the seasonal shift within emission scenario Shared Socioeconomic Pathway (SSP) 2–4.5 and the bottom panel is the ensemble mean change within emission scenario SSP 5–8.5. Blue shades indicate a shift toward increasing northern hemisphere warm season (AMJJAS) drought and decreasing cold season (ONDJFM) drought, while brown shades indicate the opposite. Grid cells where less than a majority of GCMs produce seasonal shift in the occurrence of drought greater than ±5% are shaded gray with cross-hatching.

four emission scenarios. These five storylines are, as shown in Figure 1 (S1) negative trend in total annual runoff paired with an increases in multi-year drought frequency (S2) negative trend in total annual runoff paired with an increase in the severity of annual SDI (S3) no detectable trend in total annual runoff paired with a seasonal shift in the timing of drought (S4) no detectable trend in total annual runoff paired with an increase in multi-year drought frequency, and (S5) a positive trend in total annual runoff paired with a seasonal shift in the timing of drought.

3.2. Storyline 1—Negative Runoff Trend and an Increase in Multi-Drought Frequency

Storyline 1 leads to the most frequent periods of water stress due to long-term declines in the amount of runoff available paired with more frequent multi-year drought. Regions impacted by this storyline show multiple features of extended climatological drying driven by changes to the balance of evaporative demand and precipitation (T. Wang et al., 2021) and an increase in the frequency of soil moisture deficits (Cook et al., 2020). Northern and southern South America, the Mediterranean, Central America, the central Rocky Mountain region of North America, and the Middle East are the regions at the highest risk of S1 future conditions, particularly under higher-emission scenarios (Figures 6c and 6d). Under the lower emission scenarios, SSP 1–2.6 and 2–4.5, S1 is present for a small percentage of the land area (0.1%–1.3% respectively; Table 1). As emission scenario increases in

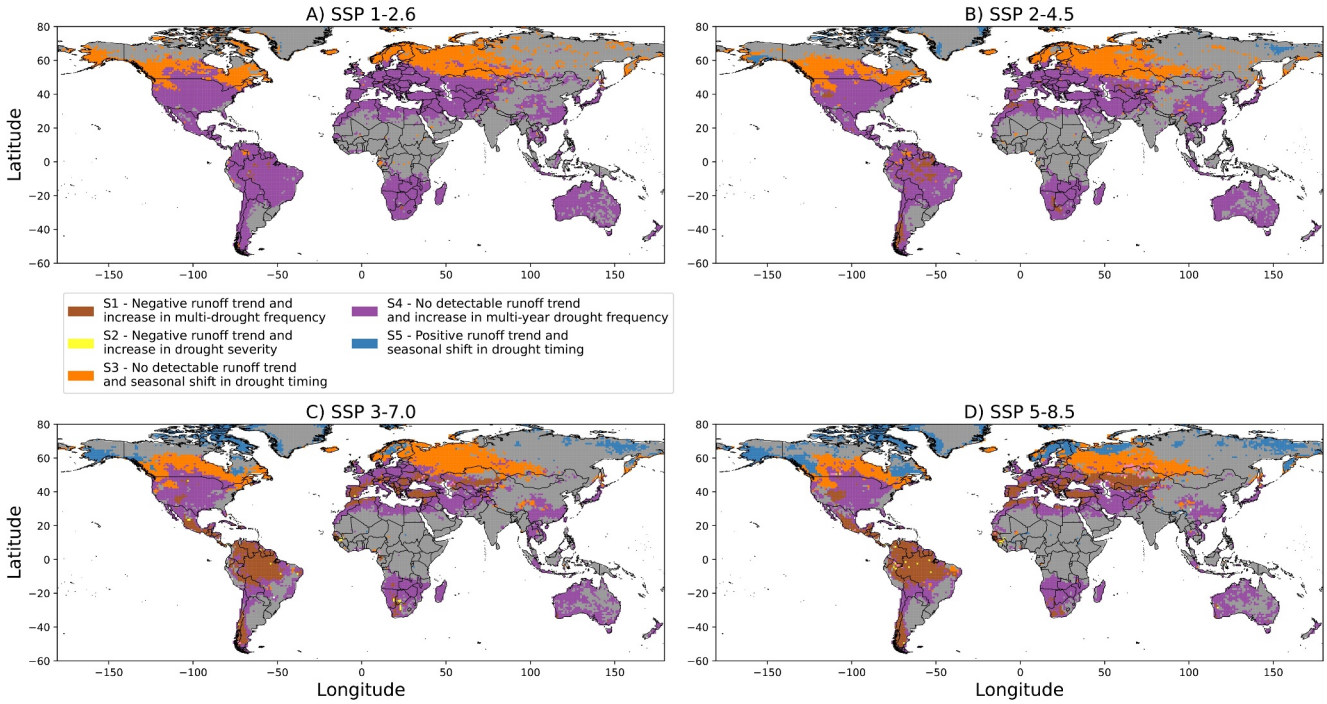

Figure 6. Dominant drought storylines across all four Shared Socioeconomic Pathways. Each panel of the figure shows the dominant storyline for the within CMIP6-MME for grid cells in the common grid for a single emission scenario. A grid cell is colored by either one of five categories of dominant storylines that are shown in (Figure 1) or gray where no one storyline is demonstrated amongst the majority of models.

severity, so too does the percentage of the land area where S1 is the dominant storyline, 5.3%–6.9% for SSPs 3–7.0–5–8.5 respectively (Figure 8). The increase in the extent of S1 under these high emission scenarios is due to a transition away from S3 within low-emission scenarios, driven by a majority of the GCMs agreeing on a shift to negative long-term runoff trends. S1 frequently occurs with S2 as its secondary storyline (Figure 7) under high emission scenarios, which suggests the changes to the water-energy balance that are driving increased frequency

Table 1
Percentage of the Total Land Area That Each Storyline is the Dominant Storyline Across the CMIP6-MME

		Future emission scenario (SSP)			
		Lower emission scenarios		Higher emission scenarios	
Storyline	Storyline features	1–2.6	2–4.5	3–7.0	5–8.5
S1	Negative runoff trend and an increase in multi-drought frequency	0.1	1.3	5.3	6.9
S2	Negative runoff trend and an increase in drought severity	0	0	0.1	0.1
S3	No detectable runoff trend and a seasonal shift in drought timing	11.1	10.2	8.9	7.3
S4	No detectable runoff trend and an increase in multi-year drought frequency	29.1	25.6	18.6	16.3
S5	Positive runoff trend and seasonal shift in drought timing	0.1	2.0	4.6	7.6

Note. For each of the five dominant storylines we report the percentage of the land-surface that is the most likely in terms of model agreement. The storylines are included for each row of the table, labeled as "S" followed by an integer than indicates the storyline. For each combination of storyline and emission scenario, the percentage of the land-surface is calculated by summing the number of grid cells where that storyline is simulated by the greatest number of GCMs and dividing that value by the total land-surface area, then multiplying by 100 to achieve a percentage.

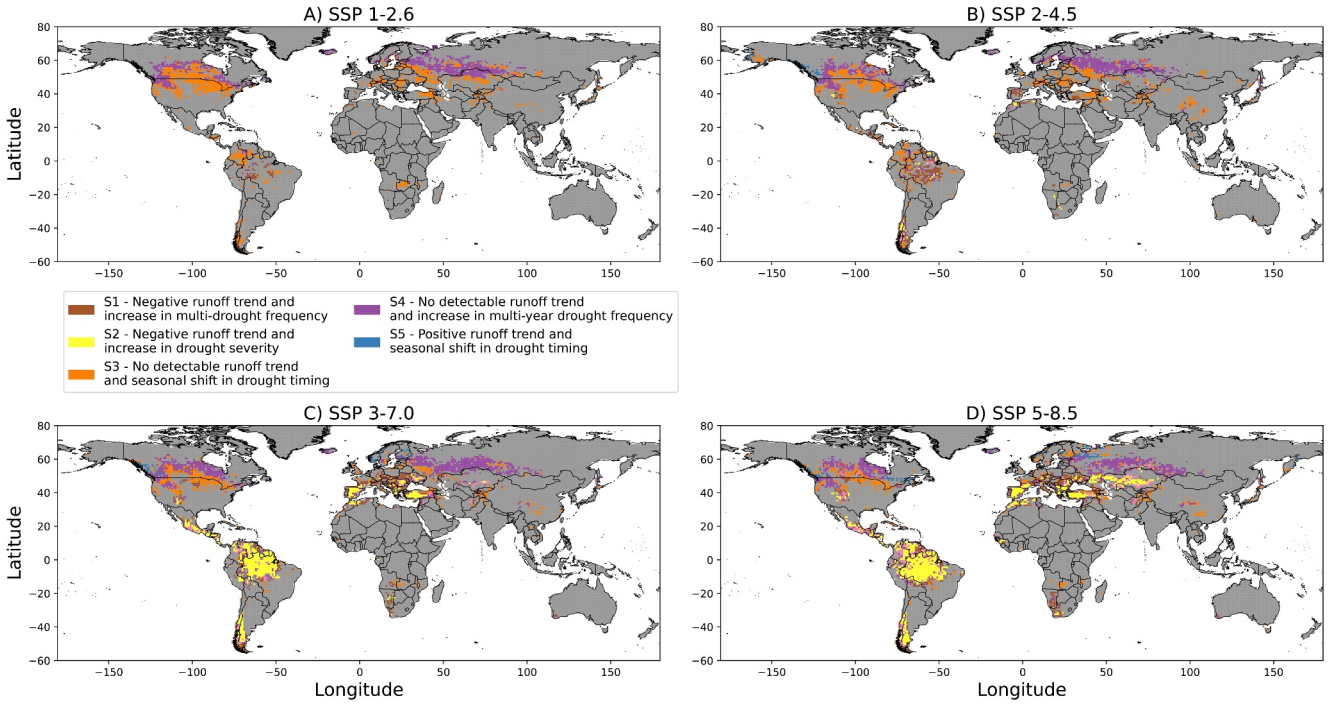

Figure 7. Secondary drought storylines across all four Shared Socioeconomic Pathways. Each panel of the figure shows the secondary storyline for the within CMIP6-MME for grid cells in the common grid for a single emission scenario. A grid cell is colored by either one of five categories of dominant storylines that are shown in Figure 1 or gray where no one storyline is demonstrated amongst the majority of models.

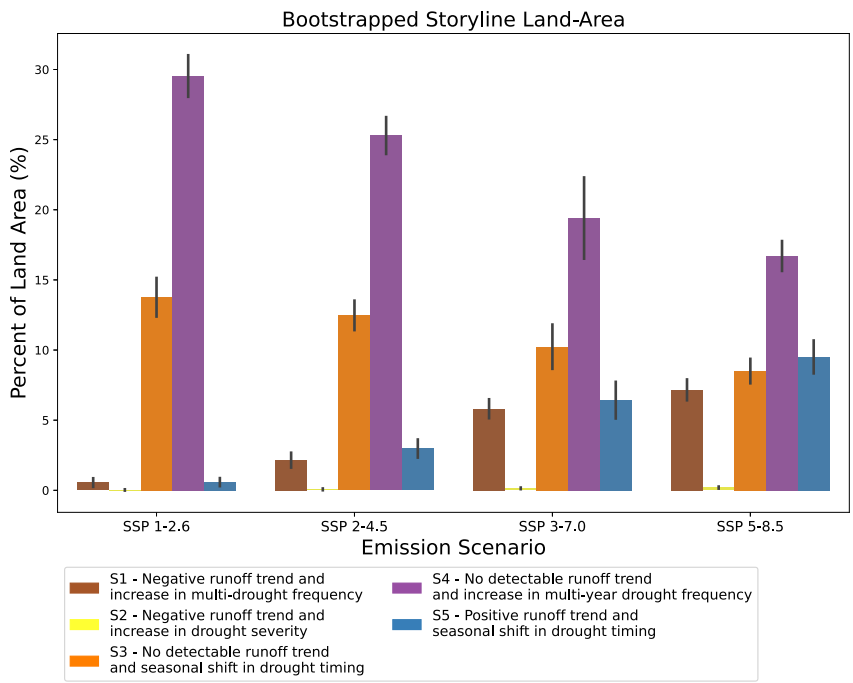

Figure 8. Percentage of the global land area that experiences each dominant storyline within a bootstrapped-resampled ensemble. The percentage of the total land-area (vertical axis) that experiences dominant storylines 1–5 (differentiated by color) for each of the four emission scenarios (horizonal axis). The height of each bar is the mean percentage of the land-area for that dominant storyline-emission scenario combination across all 500 bootstrap-resampled ensembles (described in Section 2.1). The black line in the top-middle of each bar indicates the uncertainty bounds quantified as ±1 standard-deviation from the mean of percent of land area values from all bootstrap-resampled ensemble members.

of multi-drought and negative runoff trends are also increasing the severity of annual drought, just with slightly less model consensus.

3.3. Storyline 2—Negative Runoff Trend and an Increase in Drought Severity

Storyline 2 is another of the most stressing storylines in terms of available surface water. Long-term declines in long-term runoff are driven by declines in precipitation (Orlowsky & Seneviratne, 2013; Páscoa et al., 2017; X. Zhang et al., 2007) or increases in evapotranspiration (T. Wang et al., 2021). Increases in annual drought severity arise from pronounced annual precipitation deficits coinciding with an increase to the magnitude of inter-annual precipitation variability (H. Chen & Xu, 2020; B. Zhang & Soden, 2019) or soil moisture deficits exacerbating hydrologic drought further (Cook et al., 2021). S2 only appears as the dominant storyline for 0.1% of the total land-area under the higher future emission scenarios (Table 1 and Figure 6). This is because S2 most frequently has a model consensus that is slightly lower than that of S1 and, as such, is most often a secondary storyline. S2 is a secondary storyline to S1 for 2.4%–3.4% of the land-area under SSPs 3–7.0 and 5–8.5 respectively (Table 1). The presence of S2 as a secondary storyline to S1 is most extensive in South America, the Mediterranean, the Middle East, and, to a lesser extent, the intermountain west of North America (Figure 7).

3.4. Storyline 3—No Detectable Runoff Trend and a Seasonal Shift in Drought Timing

Storyline 3 is the first storyline where the combined changes to the features of drought do not clearly lead to more frequent water-stress on the annual or decadal time scale, but rather suggest seasonal changes to the timing of water stress. S3, appearing across all emission scenarios, may be indicative of a decline in the fraction of precipitation that falls as snow in a warmer future (Cohen et al., 2015; Mote et al., 2018; Whitfield & Shook, 2020) and snowmelt occurring earlier in the year (Barnhart et al., 2020; Christianson & Johnson, 2020; McCabe & Clark, 2005). This change in the phase of precipitation can lead to cold seasons that are wetter in terms of surface runoff due, in part, to a reduction in the temporal transfer surface water from the cold to warm season through snowmelt. In warmer climates where S3 occurs, seasonal shifts in the timing of drought are driven by shifts in the timing of seasonal precipitation, such as monsoonal rains (Katzenberger et al., 2021; Park et al., 2020). In regions where S3 is the dominant storyline, the change is primarily a shift toward more frequent warm-season droughts in the northern hemisphere (Figure 6). S3 is a dominant storyline across higher northern latitudes (>40°N), while also appearing as the dominant storyline within small regions of eastern Asia. Under the lowest emission scenario, SSP 1–2.6, 11.1% of the land-surface is simulated to experience S3 as the dominant storyline, decreasing to 7.3% of the land-surface under SSP 5–8.5 (Table 1 and Figure 8). This decline in the percentage of land that experiences S3 under higher emission scenarios is due to other storylines surpassing S3 as the dominant storyline. In the high-latitudes, ensemble consensus on a positive runoff trend transitions the dominant storyline to S5, while in the mid-latitudes, a shift to model consensus on negative runoff trends and increases in multi-year drought frequency leads to S1 becoming the dominant storyline (Figures 6a–6d). Also, in the northern mid-latitudes (40–60°N), S3 is the secondary storyline to S4 along the boundary of the area that two storylines meet (Figure 7). This suggests that in northern regions with no-detectable runoff trend there is a transition zone where a shift in the timing of seasonal drought becomes the dominant storyline over an increase in multi-year drought frequency as one moves northward into colder climates.

3.5. Storyline 4—No Detectable Runoff Trend and an Increase in Multi-Year Drought Frequency

Storyline 4 is the most widespread storyline present across all emission scenarios. It occurs where there are no detectable long-term trends, but multi-year droughts become increasingly frequent in the future. S4 suggests that drought persistence becomes more frequent driven by deficits in soil moisture leading to longer duration hydrologic droughts (Cook et al., 2021; Zhao & Dai, 2022) or more frequent multi-year precipitation deficits (Seager & Hoerling, 2014). Despite more frequent multi-year drought, regions where S4 is the dominant storyline do not have detectable long-term projected trends in runoff which means that potential changes to climatological evaporative demand or precipitation do not produce a runoff trend signal that emerges outside the natural runoff variability within each simulation. The amount of land-area that has S4 as the dominant storyline shrinks as emission scenario increases, with S4 as the dominant storyline for 29.1% of the land-surface under SSP 1%–2.6% and 16.3% of the land-area under SSP 5–8.5 (Table 1). This decline is similar to that shown for S3, as the dominant storyline transitions away from S4 to storylines that include negative runoff trends under higher emission scenarios (Figures 6 and 8). Northern and southern South America, the Mediterranean, Central America,

the central Rocky Mountain region of North America, and the Middle East are all regions that have S4 as the dominant storylines that demonstrate the shift toward negative runoff trend storylines under high emission scenarios. Southern and northern Africa, much of Australia, central North America, and China also produce a majority consensus on the S4 storyline within the CMIP6-MME. However, these regions do not have a transition in the majority model consensus from no-detectable trend to a negative runoff trend that is dependent on emission scenario.

3.6. Storyline 5—Positive Runoff Trend and Seasonal Shift in Drought Timing

S5 is the only dominant drought storyline within the CMIP6-MME that includes positive long-term trends in runoff production. S5 emerges as a dominant storyline in the high northern latitudes under higher emission scenarios, which suggests that the GCMs show agreement on a positive trend in runoff resulting from a greater degree of global warming in the 21st century. This increase in runoff is consistent with previous studies that have shown an increase in artic precipitation generation within CMIP6 GCMs, particularly under higher emission scenarios (McCrystall et al., 2021). Seasonal shifts in drought frequency coincide with positive runoff trends in S5 due to warmer temperatures shifting the timing of snowmelt generated runoff (Barnhart et al., 2020; Christianson & Johnson, 2020; McCabe & Clark, 2005), consistent with S3. S5 is only present as a dominant storyline for 0.1% of the land area in the lowest emission scenario (SSP 1–2.6) (Figure 6; Table 1) and becomes the dominant storyline for a maximum of 7.6% of the land-surface under the highest emission scenario. The western coast and northeast of Canada, the Alaskan peninsula, coastal Greenland, and northern Eurasia are the regions where S5 is simulated as the dominant storyline under SSP 5–8.5. The presence of a seasonal shift in the timing of drought paired with a long-term runoff trend suggests that, while projections agree that there will be more surface water in the future period, shifts in the timing of surface water generation (Kouki et al., 2022) leave the warm-season with more frequent anomalously dry periods than experienced in the historical period.

3.7. Secondary Storylines

Secondary storylines should be considered in addition to the dominant as they represent a majority model consensus and can give insight into where storylines are geographically transitioning. Secondary storylines provide evidence that some regions would benefit from water-resource planning that includes the measures to adapt to multiple future drought storylines. Two clear dominant storyline regions with coinciding secondary storylines emerge in this analysis. The first is the northern mid-latitudes across most of North America and central Eurasia, where the increase in multi-year drought (S4) is dominant to the south and changes to seasonal timing (S3) are dominant to the north. In this region, S3–S4 are the secondary storylines to each other as the dominant storyline. This demonstrates that a shift toward colder climates in the north coincides with a change in the risk of which feature is more likely in terms of model consensus, but also that there is a transition zone at particular risk of both storylines.

Another emergence of secondary storylines extends across the Mediterranean, Middle East, Central America and South America under the highest emission scenario, where S2 is the secondary storyline to S1, which occurs for 49% of the S1 storyline grid cells globally in SSP 5–8.5. In these regions, higher emission scenarios not only include a transition toward a negative trend in runoff paired with increasingly frequent multi-year drought, but also an increase in the severity of annual drought. S2 is the secondary storyline to S1 for as much as 63% of the land-area within the Amazon River basin and 59% in the Mediterranean in SSP 5–8.5 (Figures 6 and 7), which suggests that these regions produce a frequent pairing of the storylines than the global average. The co-occurrence S1–S2 in these regions is consistent with previous analyses that have shown CMIP6 GCMs to produce negative precipitation trends and increases in the frequency of meteorological drought under high emission scenarios for both the Amazon (IPCC, 2021; Parsons, 2020) and the Mediterranean (Ukkola et al., 2020) regions. The combination of S1–S2 has the potential to significantly reduce available surface water and extend the amount of time that global regions impacted spend in water stress, which will only amplify as negative runoff trends persist through the 21st century.

3.8. Implications

Storylines that include increases in the frequency of multi-year drought (S1–S4 combined) are the most common amongst across all emission scenarios, with 29.2%–23.2% of the land surface experience experiencing these

storylines for lowest and highest emission scenarios respectively. In the absence of detectable runoff trends through the 21st century under S4, increases to the frequency of multi-year drought could yield decadal periods of water shortage that are as detrimental to water resource management, particularly for regions which are climatologically water-stressed (H. Li et al., 2021). In the presence of a long-term negative trend in runoff under higher emission scenarios, the emergence of S1 can lead to extended dry periods that can even further stress water resources for these regions. Water resource systems that rely on reservoir storage to alleviate water shortages on the interannual or decadal time scales could be vulnerable to the widespread presence of both S1–S4 under future emission scenarios if adaptation strategies to more frequent multi-droughts are not adopted (Rajagopalan et al., 2009).

Storylines that include a seasonal shift in drought timing (S3–S5) are, in part, also sensitive to the emission scenario within the CMIP6-MME. Under higher emissions, a subset of the regions that experience S3 transitioned to S5 due to ensemble consensus on a positive runoff trend. While this transition to a positive runoff trend has the potential to alleviate water stress to some degree, the presence of a shift in the seasonal timing of drought can still impact water management. For example, if seasonal droughts become more frequent during periods where water managers have historical expected a climatological influx of surface water, then that can lead short term shortages which can be broadly impactful (Christian et al., 2021; Christian-Smith et al., 2015; McNeeley et al., 2016). The spatial pattern of S3 in particular resembles that of the boreal forest extent in the northern hemisphere (Song et al., 2021), which may suggest that vegetation could be driving changes to the water-energy balance that cause seasonal drought shifts, but further investigation into the simulated vegetation feedbacks is warranted.

3.9. Limitations and Uncertainty

While storylines, as applied here, have utility in potentially simplifying our interpretation of co-occurring changes to drought features, the method has several inherent limitations. Firstly, structural similarities between GCMs in CMIP6 that persist from previous generations of models could erroneously impact the likelihood of individual storylines becoming dominant (Knutti et al., 2013). In other words, the underlying numerical representation and approximation of the physical processes could be related across GCMs such that they are not independent from each other, producing similar regional changes to drought features. This challenge exists within any analysis that considers model consensus (Knutti et al., 2013) and is thusly not alleviated with the use of storylines. Model dependent uncertainties also lead to a situation where the degree of model consensus can differ from one analysis to another simply due to the list of ensemble members (Bjarke & Gutzler, 2023; Brunner et al., 2020; Knutti et al., 2017). To estimate the sensitivity of the dominant storylines to the specific GCMs included within the ensemble, bootstrap resampling was applied to demonstrate uncertainty in the percent of the land-area that experiences each storyline (Figure 8). The percent of the land area that experiences each storyline varies within the bootstrapped ensembles by approximately 2%–5% within one standard deviation of the mean. The coefficient of variation of each storyline (Table S3 in Supporting Information S1) provides the insight that there is less relative uncertainty in the dominant storylines that cover a larger percentage of the land area. This suggests that the dominance of these storylines results from regionally consistent drought changes that are less sensitive to specific set of GCMs included in the ensemble.

Uncertainties resulting from biases in hydrologic fluxes simulated by GCMs (H. Chen & Xu, 2020; Dong et al., 2020; Lehner et al., 2019) are treated here by classifying storylines based on the directional changes in the features of drought and the sign of statistically significant runoff trends. Previous studies have shown that GCM simulations often have biases in the magnitude of hydrologic fluxes (Cook et al., 2020; Marvel et al., 2019) as well as the fidelity natural variability and extremes compared to observations (H. Chen & Xu, 2020; Cook et al., 2020; Moon et al., 2018; Pendergrass, 2020). Biases in simulated precipitation, the primary driver of runoff, arise in CMIP6 GCM simulations in part due to the parameterization of convective precipitation generation which has been shown to induce small magnitude precipitation events, that is, drizzle, more frequently than in observations (D. Chen et al., 2021; J. Li et al., 2021). These biases in the frequency of precipitation events have the potential to influence the distribution of simulated runoff and could introduce error in the analysis of GCM runoff on the seasonal to annual time scale. Differences in the distribution of simulated runoff could introduce biases into the historical baseline calculation of the frequency of drought, but this is partially treated with the use of SDI, which is calculated relative to each model's historical run.

Other uncertainties related to model sensitivity should be considered when using an ensemble of GCMs for hydroclimate analyses. Differences among GCMs in the net response to the projected future increase in surface net radiation, causes some models to produce global warming rates much higher than others (Brunner et al., 2020; Pendergrass, 2020). These sensitivity differences may result in biases in ensemble behavior caused by models with large, often unrealistic, degrees of warming response and more extreme changes in hydrologic fluxes when compared to changes observed in the historical period (Brunner et al., 2020; Dong et al., 2020; Lehner et al., 2019; Pendergrass, 2020; Zelinka et al., 2020). There are also differences between the GCMs in the sensitivities of their land-surface response to changes in temperatures and precipitation that can generate biases in future runoff production (Lehner et al., 2019). An alternative approach is to use downscaled, bias corrected meteorological outputs from GCMs as forcings for an offline hydrologic model, but this introduces other uncertainties into the analysis related to individual hydrologic model sensitivities (Vano et al., 2012) and a lack of land-atmosphere coupling.

Finally, we only considered three features and long term runoff trends in this analysis, but there are other drought features related to the hydroclimate that are of interest, such as agricultural drought (Cook et al., 2021), snow drought (Heldmyer et al., 2023), or heatwaves (Mazdiyasni & AghaKouchak, 2015), that could be included in a more extensive list of drought storylines. Here we offer a small subset of potential drought storyline permutations that directly relate to surface water availability and that may be useful for water resource planning. Furthermore, it is possible that grid cells can experience opposite changes to the features of drought that would alleviate stress to water resource systems, such as a decrease in multi-year drought frequency or a decrease in the severity of average annual drought. Along these lines, one could apply this methodology to determine storylines of drought alleviation, or even flooding, but we are specifically interested in evaluating where drought storylines can help inform water resource managers for future shortages on seasonal to multi-annual time scales.

4. Conclusions

This work is motivated by the need to further understand how multiple drought features are projected to change across the global land-surface and how they relate to long-term changes to available surface water. We address this need by using the storyline framework to provide evidence of where plausible changes to the features of drought (Shepherd et al., 2018) find consensus among CMIP6 simulations. We provide examples of how storylines can be used to identify regions that are at risk of stressed surface water resources due to changes in the features of drought, including increased drought severity, higher frequency of multi-year drought, and shifts in the seasonal timing of drought.

The presence of multiple dominant drought storylines that can stress water resources across all emission scenarios suggests that some degree of climate change induced hydrologic drought enhancements are likely unavoidable. A majority of models reach a consensus on future storylines that involve an increase in the frequency of multi-year hydrologic drought across nearly a third of the global land-surface, even under the lowest emission scenario. Furthermore, high latitudes exhibit dominant storylines that involve a seasonal shift in the timing of drought for all future emission scenarios. The presence of these dominant drought storylines in the CMIP6 ensemble suggests that, even under the most significant emission reduction pathways, drought features are likely to change in a manner that will necessitate adaptation of water resources.

Under higher emission scenarios and greater warming, we observe an expansion in the area of the land-surface experiencing dominant storylines that involve long-term runoff declines. These storylines pair negative runoff trends with both an increase in the frequency of multi-year drought and an increase in drought severity, leading to the worst-case scenario in terms of water stress. The increasing dominance of these storylines under the highest emission scenario serves as a call to action for proactive management of water resources throughout the 21st century.

Data Availability Statement

All data derived from the CMIP6 simulations used here are freely available from the Earth System Grid Federation (https://esgf-node.llnl.gov/search/cmip6/). Climate data were analyzed on the monthly temporal resolution using raw CMIP6 climate output files that are organized by variable, GCM, simulation period, scenario, and variant member. All GCMs used are referenced in the supplemental information document (Table S1

in Supporting Information S1). To demonstrate the regional agreement on storylines, the authors used the Climate Data Operators toolset (https://code.mpimet.mpg.de/projects/cdo) to remap the storylines to a common grid.

Acknowledgments
We acknowledge the funding support provided to this project through the NOAA cooperative agreements NA17OAR4320101 and NA22OAR4320151 (CIRES), as well as the NOAA MAPP Grant titled NOAA Grant NA20OAR4310420 Identifying Alternatives to Snow-based Streamflow Predictions to Advance Future Drought Predictability, NOAA Grant titled "Physically-based evaluation of CMIP6 hydrologic projections for the western United States (NA19OAR4310284) and the NOAA Grant titled": "Western Water Assessment: Building resilience to compound hazards in the Intermountain West (NA21OAR4310309) that made this research possible."

References

Anderegg, W. R. L., Hicke, J. A., Fisher, R. A., Allen, C. D., Aukema, J., Bentz, B., et al. (2015). Tree mortality from drought, insects, and their interactions in a changing climate. *New Phytologist*, *208*(3), 674–683. https://doi.org/10.1111/nph.13477

Anisimov, O. A., Vaughan, D. G., Callaghan, T. V., Furgal, C., Marchant, H., Prowse, T. D., et al. (2007). Climate change 2007: Impacts, adaptation and vulnerability. Contribution of working group II to the fourth assessment report of the intergovernmental panel on climate change. In M. L. Parry, O. F. Canziani, J. P. Palutikof, P. J. van der Linden, & C. E. Hanson (Eds.), *Polar regions (Arctic and Antarctic)* (pp. 653–685). Cambridge University Press.

Barnett, T. P., Adam, J. C., & Lettenmaier, D. P. (2005). Potential impacts of a warming climate on water availability in snow-dominated regions. *Nature*, *438*, 7066–7309. https://doi.org/10.1038/nature04141

Barnhart, T. B., Tague, C. L., & Molotch, N. P. (2020). The counteracting effects of snowmelt rate and timing on runoff. *Water Resources Research*, *56*(8), e2019WR026634. https://doi.org/10.1029/2019WR026634

Barsugli, J. J., Vogel, J. M., Kaatz, L., Smith, J. B., Waage, M., & Anderson, C. J. (2012). Two faces of uncertainty: Climate science and water utility planning methods. *Journal of Water Resources Planning and Management*, *138*(5), 389–395. https://doi.org/10.1061/(asce)wr.1943-5452.0000188

Berg, N., & Hall, A. (2017). Anthropogenic warming impacts on California snowpack during drought. *Geophysical Research Letters*, *44*(5), 2511–2518. https://doi.org/10.1002/2016GL072104

Bjarke, N., Barsugli, J., & Livneh, B. (2023). CMIP6 derived ensemble of global vapor pressure deficit, potential evapotranspiration, and reference evapotranspiration [Dataset]. *Zenodo*. https://doi.org/10.5281/ZENODO.7789759

Bjarke, N. R., & Gutzler, D. S. (2023). Use of observed Hydroclimatic trends to constrain projections of snowmelt season runoff in the Rio Grande headwaters. *JAWRA Journal of the American Water Resources Association*, *59*(5), 1025–1040. https://doi.org/10.1111/1752-1688.13118

Brown, C., Steinschneider, S., Ray, P., Wi, S., Basdekas, L., & Yates, D. (2019). Decision Scaling (DS): Decision support for climate change. In V. A. W. J. Marchau, W. E. Walker, P. J. T. M. Bloemen, & S. W. Popper (Eds.), *Decision making under deep uncertainty: From theory to practice* (pp. 255–287). Springer International Publishing. https://doi.org/10.1007/978-3-030-05252-2_12

Brunner, L., Pendergrass, A. G., Lehner, F., Merrifield, A. L., Lorenz, R., & Knutti, R. (2020). Reduced global warming from CMIP6 projections when weighting models by performance and independence. *Earth System Dynamics*, *11*(4), 995–1012. https://doi.org/10.5194/esd-11-995-2020

Budescu, D. V., Por, H.-H., & Broomell, S. B. (2012). Effective communication of uncertainty in the IPCC reports. *Climatic Change*, *113*(2), 181–200. https://doi.org/10.1007/s10584-011-0330-3

Campbell, J. D., Taylor, M. A., Stephenson, T. S., Watson, R. A., & Whyte, F. S. (2011). Future climate of the Caribbean from a regional climate model. *International Journal of Climatology*, *31*(12), 1866–1878. https://doi.org/10.1002/joc.2200

Carlton, J. S., Mase, A. S., Knutson, C. L., Lemos, M. C., Haigh, T., Todey, D. P., & Prokopy, L. S. (2016). The effects of extreme drought on climate change beliefs, risk perceptions, and adaptation attitudes. *Climatic Change*, *135*(2), 211–226. https://doi.org/10.1007/s10584-015-1561-5

Cayan, D. R., Das, T., Pierce, D. W., Barnett, T. P., Tyree, M., & Gershunov, A. (2010). Future dryness in the southwest US and the hydrology of the early 21st century drought. *Proceedings of the National Academy of Sciences*, *107*(50), 21271–21276. https://doi.org/10.1073/pnas.0912391107

Chan, W. C., Shepherd, T. G., Facer-Childs, K., Darch, G., & Arnell, N. W. (2022). Storylines of UK drought based on the 2010–2012 event. *Hydrology and Earth System Sciences*, *26*(7), 1755–1777. https://doi.org/10.5194/hess-26-1755-2022

Chen, D., Dai, A., & Hall, A. (2021). The convective-to-total precipitation ratio and the "Drizzling" bias in climate models. *Journal of Geophysical Research*, *126*(16), e2020JD034198. https://doi.org/10.1029/2020JD034198

Chen, H., & Xu, Z. (2020). Decadal-to-multidecadal variability of seasonal land precipitation in Northern Hemisphere in observation and CMIP6 historical simulations. *Atmosphere*, *11*(2), 195. https://doi.org/10.3390/atmos11020195

Chen, L. G., Gottschalck, J., Hartman, A., Miskus, D., Tinker, R., & Artusa, A. (2019). Flash drought characteristics based on US drought monitor. *Atmosphere*, *10*(9), 498. https://doi.org/10.3390/atmos10090498

Christian, J. I., Basara, J. B., Hunt, E. D., Otkin, J. A., Furtado, J. C., Mishra, V., et al. (2021). Global distribution, trends, and drivers of flash drought occurrence. *Nature Communications*, *12*(1), 6330. https://doi.org/10.1038/s41467-021-26692-z

Christian, J. I., Basara, J. B., Otkin, J. A., Hunt, E. D., Wakefield, R. A., Flanagan, P. X., & Xiao, X. (2019). A methodology for flash drought identification: Application of flash drought frequency across the United States. *Journal of Hydrometeorology*, *20*(5), 833–846. https://doi.org/10.1175/jhm-d-18-0198.1

Christian-Smith, J., Levy, M. C., & Gleick, P. H. (2015). Maladaptation to drought: A case report from California, USA. *Sustainability Science*, *10*(3), 491–501. https://doi.org/10.1007/s11625-014-0269-1

Christianson, K. R., & Johnson, B. M. (2020). Combined effects of early snowmelt and climate warming on mountain lake temperatures and fish energetics. *Arctic Antarctic and Alpine Research*, *52*(1), 130–145. https://doi.org/10.1080/15230430.2020.1741199

Ciais, P. H., Reichstein, M., Viovy, N., Granier, A., Ogée, J., Allard, V., et al. (2005). Europe-wide reduction in primary productivity caused by the heat and drought in 2003. *Nature*, *437*(7058), 529–533. https://doi.org/10.1038/nature03972

Cline, D. W. (1997). Snow surface energy exchanges and snowmelt at a continental, midlatitude Alpine site. *Water Resources Research*, *33*(4), 689–701. https://doi.org/10.1029/97WR00026

Coats, S., Smerdon, J. E., Cook, B. I., & Seager, R. (2013). Stationarity of the tropical Pacific teleconnection to North America in CMIP5/PMIP3 model simulations. *Geophysical Research Letters*, *40*(18), 4927–4932. https://doi.org/10.1002/grl.50938

Cohen, J., Ye, H., & Jones, J. (2015). Trends and variability in rain-on-snow events. *Geophysical Research Letters*, *42*(17), 7115–7122. https://doi.org/10.1002/2015GL065320

Cook, B. I., Mankin, J. S., Marvel, K., Williams, A. P., Smerdon, J. E., & Anchukaitis, K. J. (2020). Twenty-first century drought projections in the CMIP6 forcing scenarios. *Earth's Future*, *8*(6), e2019EF001461. https://doi.org/10.1029/2019EF001461

Cook, B. I., Mankin, J. S., Williams, A. P., Marvel, K. D., Smerdon, J. E., & Liu, H. (2021). Uncertainties, limits, and benefits of climate change mitigation for soil moisture drought in Southwestern North America. *Earth's Future*, *9*(9), e2021EF002014. https://doi.org/10.1029/2021EF002014

Dessai, S., & Hulme, M. (2004). Does climate adaptation policy need probabilities? *Climate Policy*, *4*(2), 107–128. https://doi.org/10.1080/14693062.2004.9685515

Dong, Y., Armour, K. C., Zelinka, M. D., Proistosescu, C., Battisti, D. S., Zhou, C., & Andrews, T. (2020). Intermodel spread in the pattern effect and its contribution to climate sensitivity in CMIP5 and CMIP6 models. *Journal of Climate*, *33*(18), 7755–7775. https://doi.org/10.1175/jcli-d-19-1011.1

Eyring, V., Bony, S., Meehl, G. A., Senior, C. A., Stevens, B., Stouffer, R. J., & Taylor, K. E. (2016). Overview of the Coupled Model Intercomparison Project Phase 6 (CMIP6) experimental design and organization. *Geoscientific Model Development*, *9*(5), 1937–1958. https://doi.org/10.5194/gmd-9-1937-2016

Frederick, K. D., & Major, D. C. (1997). Climate change and water resources. *Climatic Change*, *37*(1), 7–23. https://doi.org/10.1007/978-94-017-1051-0_2

Garreaud, R. D., Boisier, J. P., Rondanelli, R., Montecinos, A., Sepúlveda, H. H., & Veloso-Aguila, D. (2020). The Central Chile mega drought (2010–2018): A climate dynamics perspective. *International Journal of Climatology*, *40*(1), 421–439. https://doi.org/10.1002/joc.6219

Gessner, C., Fischer, E. M., Beyerle, U., & Knutti, R. (2022). Multi-year drought storylines for Europe and North America from an iteratively perturbed global climate model. *Weather and Climate Extremes*, *38*, 100512. https://doi.org/10.1016/j.wace.2022.100512

Goulart, H. M., Van Der Wiel, K., Folberth, C., Balkovic, J., & Van Den Hurk, B. (2021). Storylines of weather-induced crop failure events under climate change. *Earth System Dynamics*, *12*(4), 1503–1527. https://doi.org/10.5194/esd-12-1503-2021

Heim, R. R., Jr. (2002). A review of twentieth-century drought indices used in the United States. *Bulletin of the American Meteorological Society*, *83*(8), 1149–1166. https://doi.org/10.1175/1520-0477-83.8.1149

Heldmyer, A. J., Bjarke, N. R., & Livneh, B. (2023). A 21st-century perspective on snow drought in the Upper Colorado River Basin. *JAWRA Journal of the American Water Resources Association*, *59*(2), 396–415. https://doi.org/10.1111/1752-1688.13095

Herrando-Pérez, S., Bradshaw, C. J., Lewandowsky, S., & Vieites, D. R. (2019). Statistical language backs conservatism in climate-change assessments. *BioScience*, *69*(3), 209–219. https://doi.org/10.1093/biosci/biz004

Hoell, A., Perlwitz, J., Dewes, C., Wolter, K., Rangwala, I., Quan, X.-W., & Eischeid, J. (2019). Anthropogenic contributions to the intensity of the 2017 United States Northern Great Plains drought. *Bulletin of the American Meteorological Society*, *100*(1), S19–S24. https://doi.org/10.1175/BAMS-D-18-0127.1

Hoerling, M., Eischeid, J., Perlwitz, J., Quan, X., Zhang, T., & Pegion, P. (2012). On the increased frequency of Mediterranean drought. *Journal of Climate*, *25*(6), 2146–2161. https://doi.org/10.1175/JCLI-D-11-00296.1

IPCC. (2021). Climate change 2021: The physical science basis. In V. Masson-Delmotte, P. Zhai, A. Pirani, S. L. Connors, C. Péan, et al. (Eds.), *Contribution of Working Group I to the Sixth Assessment Report of the Intergovernmental Panel on Climate Change*. Cambridge University Press.

Jiang, Z., Johnson, F., & Sharma, A. (2023). Do derived drought indices better characterize future drought change? *Earth's Future*, *11*(7), e2022EF003350. https://doi.org/10.1029/2022EF003350

Katzenberger, A., Schewe, J., Pongratz, J., & Levermann, A. (2021). Robust increase of Indian monsoon rainfall and its variability under future warming in CMIP6 models. *Earth System Dynamics*, *12*(2), 367–386. https://doi.org/10.5194/esd-12-367-2021

King, A. D., Pitman, A. J., Henley, B. J., Ukkola, A. M., & Brown, J. R. (2020). The role of climate variability in Australian drought. *Nature Climate Change*, *10*(3), 177–179. https://doi.org/10.1038/s41558-020-0718-z

Knutti, R., Masson, D., & Gettelman, A. (2013). Climate model genealogy: Generation CMIP5 and how we got there: Climate model genealogy. *Geophysical Research Letters*, *40*(6), 1194–1199. https://doi.org/10.1002/grl.50256

Knutti, R., Sedláček, J., Sanderson, B. M., Lorenz, R., Fischer, E. M., & Eyring, V. (2017). A climate model projection weighting scheme accounting for performance and interdependence. *Geophysical Research Letters*, *44*(4), 1909–1918. https://doi.org/10.1002/2016GL072012

Kouki, K., Räisänen, P., Luojus, K., Luomaranta, A., & Riihelä, A. (2022). Evaluation of Northern Hemisphere snow water equivalent in CMIP6 models during 1982–2014. *The Cryosphere*, *16*(3), 1007–1030. https://doi.org/10.5194/tc-16-1007-2022

Kundzewicz, Z. W., Mata, L., Arnell, N. W., Döll, P., Jimenez, B., Miller, K., et al. (2008). The implications of projected climate change for freshwater resources and their management. *Hydrological Sciences Journal*, *53*(1), 3–10. https://doi.org/10.1623/hysj.53.1.3

Lehner, F., Wood, A. W., Vano, J. A., Lawrence, D. M., Clark, M. P., & Mankin, J. S. (2019). The potential to reduce uncertainty in regional runoff projections from climate models. *Nature Climate Change*, *9*(12), 926–933. https://doi.org/10.1038/s41558-019-0639-x

Leonard, M., Westra, S., Phatak, A., Lambert, M., van den Hurk, B., McInnes, K., et al. (2014). A compound event framework for understanding extreme impacts. *WIREs Climate Change*, *5*(1), 113–128. https://doi.org/10.1002/wcc.252

Li, H., Li, Z., Chen, Y., Xiang, Y., Liu, Y., Kayumba, P. M., & Li, X. (2021). Dryland face potential threat of robust drought in the CMIP6 SSPs scenarios. *Environmental Research Letters*, *16*(11), 114004. https://doi.org/10.1088/1748-9326/ac2bce

Li, J., Miao, C., Wei, W., Zhang, G., Hua, L., Chen, Y., & Wang, X. (2021). Evaluation of CMIP6 global climate models for simulating land surface energy and water fluxes during 1979–2014. *Journal of Advances in Modeling Earth Systems*, *13*(6), e2021MS002515. https://doi.org/10.1029/2021MS002515

Lian, X., Piao, S., Huntingford, C., Li, Y., Zeng, Z., Wang, X., et al. (2018). Partitioning global land evapotranspiration using CMIP5 models constrained by observations. *Nature Climate Change*, *8*(7), 640–646. https://doi.org/10.1038/s41558-018-0207-9

Marvel, K., Cook, B. I., Bonfils, C. J. W., Durack, P. J., Smerdon, J. E., & Williams, A. P. (2019). Twentieth-century hydroclimate changes consistent with human influence. *Nature*, *569*(7754), 59–65. https://doi.org/10.1038/s41586-019-1149-8

Mazdiyasni, O., & AghaKouchak, A. (2015). Substantial increase in concurrent droughts and heatwaves in the United States. *Proceedings of the National Academy of Sciences of the United States of America*, *112*(37), 11484–11489. https://doi.org/10.1073/pnas.1422945112

McCabe, G. J., & Clark, M. P. (2005). Trends and variability in snowmelt runoff in the western United States. *Journal of Hydrometeorology*, *6*(4), 476–482. https://doi.org/10.1175/jhm428.1

McCabe, G. J., Wolock, D. M., Pederson, G. T., Woodhouse, C. A., & McAfee, S. (2017). Evidence that recent warming is reducing upper Colorado River flows. *Earth Interactions*, *21*(10), 1–14. https://doi.org/10.1175/EI-D-17-0007.1

McCrystall, M. R., Stroeve, J., Serreze, M., Forbes, B. C., & Screen, J. A. (2021). New climate models reveal faster and larger increases in Arctic precipitation than previously projected. *Nature Communications*, *12*(1), 6765. https://doi.org/10.1038/s41467-021-27031-y

McKee, T. B., Doesken, N. J., & Kleist, J. (1993). The relationship of drought frequency and duration to time scales. In. *Proceedings of the 8th Conference on Applied Climatology*, (Vol. 17, No. 22, pp. 179–183).

McNeeley, S. M., Beeton, T. A., & Ojima, D. S. (2016). Drought risk and adaptation in the interior United States: Understanding the importance of local context for resource management in times of drought. *Weather, Climate, and Society*, *8*(2), 147–161. https://doi.org/10.1175/wcas-d-15-0042.1

Moon, H., Gudmundsson, L., & Seneviratne, S. I. (2018). Drought persistence errors in global climate models. *Journal of Geophysical Research*, *123*(7), 3483–3496. https://doi.org/10.1002/2017JD027577

Mote, P. W., Li, S., Lettenmaier, D. P., Xiao, M., & Engel, R. (2018). Dramatic declines in snowpack in the western US. *Npj Climate and Atmospheric Science*, *1*(1), 2. https://doi.org/10.1038/s41612-018-0012-1

Nalbantis, I., & Tsakiris, G. (2009). Assessment of hydrological drought revisited. *Water Resources Management*, *23*(5), 881–897. https://doi.org/10.1007/s11269-008-9305-1

Neelin, J. D., Langenbrunner, B., Meyerson, J. E., Hall, A., & Berg, N. (2013). California winter precipitation change under global warming in the Coupled Model Intercomparison Project phase 5 ensemble. *Journal of Climate*, *26*(17), 6238–6256. https://doi.org/10.1175/jcli-d-12-00514.1

Nicholls, N. (2004). The changing nature of Australian droughts. *Climatic Change*, *63*(3), 323–336. https://doi.org/10.1023/b:clim.0000018515.46344.6d

Olmstead, S. M. (2014). Climate change adaptation and water resource management: A review of the literature. *Energy Economics*, *46*, 500–509. https://doi.org/10.1016/j.eneco.2013.09.005

O'Neill, B. C., Tebaldi, C., van Vuuren, D. P., Eyring, V., Friedlingstein, P., Hurtt, G., et al. (2016). The Scenario Model Intercomparison Project (ScenarioMIP) for CMIP6. *Geoscientific Model Development*, *9*(9), 3461–3482. https://doi.org/10.5194/gmd-9-3461-2016

Orlowsky, B., & Seneviratne, S. I. (2013). Elusive drought: Uncertainty in observed trends and short- and long-term CMIP5 projections. *Hydrology and Earth System Sciences*, *17*(5), 1765–1781. https://doi.org/10.5194/hess-17-1765-2013

Otto, F. E. L., Wolski, P., Lehner, F., Tebaldi, C., Van Oldenborgh, G. J., Hogesteeger, S., et al. (2018). Anthropogenic influence on the drivers of the Western Cape drought 2015–2017. *Environmental Research Letters*, *13*(12), 124010. https://doi.org/10.1088/1748-9326/aae9f9

Padrón, R. S., Gudmundsson, L., & Seneviratne, S. I. (2019). Observational constraints reduce likelihood of extreme changes in multidecadal land water availability. *Geophysical Research Letters*, *46*(2), 736–744. https://doi.org/10.1029/2018GL080521

Papalexiou, S. M., Rajulapati, C. R., Andreadis, K. M., Foufoula-Georgiou, E., Clark, M. P., & Trenberth, K. E. (2021). Probabilistic evaluation of drought in CMIP6 simulations. *Earth's Future*, *9*(10), e2021EF002150. https://doi.org/10.1029/2021EF002150

Park, J., Kim, H., Wang, S.-Y. S., Jeong, J.-H., Lim, K.-S., LaPlante, M., & Yoon, J.-H. (2020). Intensification of the East Asian summer monsoon lifecycle based on observation and CMIP6. *Environmental Research Letters*, *15*(9), 0940b9. https://doi.org/10.1088/1748-9326/ab9b3f

Parsons, L. A. (2020). Implications of CMIP6 projected drying trends for 21st century Amazonian drought risk. *Earth's Future*, *8*(10), e2020EF001608. https://doi.org/10.1029/2020ef001608

Páscoa, P., Gouveia, C., Russo, A., & Trigo, R. (2017). Drought trends in the Iberian Peninsula over the last 112 years. *Advances in Meteorology*, *2017*, 1–13. https://doi.org/10.1155/2017/4653126

Pendergrass, A. G. (2020). The global-mean precipitation response to CO_2-induced warming in CMIP6 models. *Geophysical Research Letters*, *47*(17), e2020GL089964. https://doi.org/10.1029/2020gl089964

Rajagopalan, B., Nowak, K., Prairie, J., Hoerling, M., Harding, B., Barsugli, J., et al. (2009). Water supply risk on the Colorado River: Can management mitigate? *Water Resources Research*, *45*(8), W08201. https://doi.org/10.1029/2008WR007652

Rajulapati, C. R., Papalexiou, S. M., Clark, M. P., & Pomeroy, J. W. (2021). The perils of regridding: Examples using a global precipitation dataset. *Journal of Applied Meteorology and Climatology*, *60*(11), 1561–1573. https://doi.org/10.1175/JAMC-D-20-0259.1

Schmidt, D. F., & Grise, K. M. (2021). Drivers of twenty-first-century US winter precipitation trends in CMIP6 models: A storyline-based approach. *Journal of Climate*, *34*(16), 6875–6889.

Seager, R., & Hoerling, M. (2014). Atmosphere and ocean origins of North American droughts. *Journal of Climate*, *27*(12), 4581–4606. https://doi.org/10.1175/jcli-d-13-00329.1

Seager, R., Osborn, T. J., Kushnir, Y., Simpson, I. R., Nakamura, J., & Liu, H. (2019). Climate variability and change of Mediterranean-type climates. *Journal of Climate*, *32*(10), 2887–2915. https://doi.org/10.1175/JCLI-D-18-0472.1

Shepherd, T. G., Boyd, E., Calel, R. A., Chapman, S. C., Dessai, S., Dima-West, I. M., et al. (2018). Storylines: An alternative approach to representing uncertainty in physical aspects of climate change. *Climatic Change*, *151*(3), 555–571. https://doi.org/10.1007/s10584-018-2317-9

Shepherd, T. G., & Lloyd, E. A. (2021). Meaningful climate science. *Climatic Change*, *169*(1–2), 17. https://doi.org/10.1007/s10584-021-03246-2

Siirila-Woodburn, E. R., Rhoades, A. M., Hatchett, B. J., Huning, L. S., Szinai, J., Tague, C., et al. (2021). A low-to-no snow future and its impacts on water resources in the western United States. *Nature Reviews Earth and Environment*, *2*(11), 800–819. https://doi.org/10.1038/s43017-021-00219-y

Song, X., Wang, D.-Y., Li, F., & Zeng, X.-D. (2021). Evaluating the performance of CMIP6 Earth system models in simulating global vegetation structure and distribution. *Advances in Climate Change Research*, *12*(4), 584–595. https://doi.org/10.1016/j.accre.2021.06.008

Srivastava, A., Grotjahn, R., & Ullrich, P. A. (2020). Evaluation of historical CMIP6 model simulations of extreme precipitation over contiguous US regions. *Weather and Climate Extremes*, *29*, 100268. https://doi.org/10.1016/j.wace.2020.100268

Tebaldi, C., Arblaster, J. M., & Knutti, R. (2011). Mapping model agreement on future climate projections. *Geophysical Research Letters*, *38*(23), L23701. https://doi.org/10.1029/2011gl049863

Ukkola, A. M., De Kauwe, M. G., Roderick, M. L., Abramowitz, G., & Pitman, A. J. (2020). Robust future changes in meteorological drought in CMIP6 projections despite uncertainty in precipitation. *Geophysical Research Letters*, *47*(11), e2020GL087820. https://doi.org/10.1029/2020GL087820

Ukkola, A. M., Pitman, A. J., De Kauwe, M. G., Abramowitz, G., Herger, N., Evans, J. P., & Decker, M. (2018). Evaluating CMIP5 model agreement for multiple drought metrics. *Journal of Hydrometeorology*, *19*(6), 969–988. https://doi.org/10.1175/JHM-D-17-0099.1

van den Hurk, B. J., Pacchetti, M. B., Boere, E., Ciullo, A., Coulter, L., Dessai, S., et al. (2023). Climate impact storylines for assessing socio-economic responses to remote events. *Climate Risk Management*, *40*, 100500. https://doi.org/10.1016/j.crm.2023.100500

Van der Schrier, G., Jones, P., & Briffa, K. (2011). The sensitivity of the PDSI to the Thornthwaite and Penman-Monteith parameterizations for potential evapotranspiration. *Journal of Geophysical Research*, *116*(D3), D03106. https://doi.org/10.1029/2010jd015001

van der Wiel, K., Lenderink, G., & de Vries, H. (2021). Physical storylines of future European drought events like 2018 based on ensemble climate modelling. *Weather and Climate Extremes*, *33*, 100350. https://doi.org/10.1016/j.wace.2021.100350

Van Dijk, A. I., Beck, H. E., Crosbie, R. S., De Jeu, R. A., Liu, Y. Y., Podger, G. M., et al. (2013). The Millennium Drought in southeast Australia (2001–2009): Natural and human causes and implications for water resources, ecosystems, economy, and society. *Water Resources Research*, *49*(2), 1040–1057. https://doi.org/10.1002/wrcr.20123

van Garderen, L., & Mindlin, J. (2022). A storyline attribution of the 2011/2012 drought in Southeastern South America. *Weather*, *77*(6), 212–218. https://doi.org/10.1002/wea.4185

Vano, J. A., Das, T., & Lettenmaier, D. P. (2012). Hydrologic sensitivities of Colorado River runoff to changes in precipitation and temperature. *Journal of Hydrometeorology*, *13*(3), 932–949. https://doi.org/10.1175/JHM-D-11-069.1

Vicente-Serrano, S. M. (2006). Spatial and temporal analysis of droughts in the Iberian Peninsula (1910–2000). *Hydrological Sciences Journal*, *51*(1), 83–97. https://doi.org/10.1623/hysj.51.1.83

Wackerly, D., Mendenhall, W., & Scheaffer, R. L. (2014). *Mathematical statistics with applications*. Cengage Learning.

Wang, A., Miao, Y., Kong, X., & Wu, H. (2022). Future changes in global runoff and runoff coefficient from CMIP6 multi-model simulation under SSP1-2.6 and SSP5-8.5 scenarios. *Earth's Future*, *10*(12), e2022EF002910. https://doi.org/10.1029/2022EF002910

Wang, T., Tu, X., Singh, V. P., Chen, X., & Lin, K. (2021). Global data assessment and analysis of drought characteristics based on CMIP6. *Journal of Hydrology*, *596*, 126091. https://doi.org/10.1016/j.jhydrol.2021.126091

Whitfield, P. H., & Shook, K. R. (2020). Changes to rainfall, snowfall, and runoff events during the autumn-winter transition in the Rocky Mountains of North America. *Canadian Water Resources Journal*, *45*(1), 28–42. https://doi.org/10.1080/07011784.2019.1685910

Williams, A. P., Seager, R., Abatzoglou, J. T., Cook, B. I., Smerdon, J. E., & Cook, E. R. (2015). Contribution of anthropogenic warming to California drought during 2012–2014. *Geophysical Research Letters*, *42*(16), 6819–6828. https://doi.org/10.1002/2015GL064924

Woodhouse, C. A., Meko, D. M., MacDonald, G. M., Stahle, D. W., & Cook, E. R. (2010). A 1,200-year perspective of 21st century drought in Southwestern North America. *Proceedings of the National Academy of Sciences*, *107*(50), 21283–21288. https://doi.org/10.1073/pnas.0911197107

Yuan, X., Wang, L., Wu, P., Ji, P., Sheffield, J., & Zhang, M. (2019). Anthropogenic shift towards higher risk of flash drought over China. *Nature Communications*, *10*(1), 4661. https://doi.org/10.1038/s41467-019-12692-7

Zeff, H. B., Herman, J. D., Reed, P. M., & Characklis, G. W. (2016). Cooperative drought adaptation: Integrating infrastructure development, conservation, and water transfers into adaptive policy pathways. *Water Resources Research*, *52*(9), 7327–7346. https://doi.org/10.1002/2016WR018771

Zelinka, M. D., Myers, T. A., McCoy, D. T., Po-Chedley, S., Caldwell, P. M., Ceppi, P., et al. (2020). Causes of higher climate sensitivity in CMIP6 models. *Geophysical Research Letters*, *47*(1), e2019GL085782. https://doi.org/10.1029/2019gl085782

Zhang, B., & Soden, B. J. (2019). Constraining climate model projections of regional precipitation change. *Geophysical Research Letters*, *46*(17–18), 10522–10531. https://doi.org/10.1029/2019GL083926

Zhang, X., Zwiers, F. W., Hegerl, G. C., Lambert, F. H., Gillett, N. P., Solomon, S., et al. (2007). Detection of human influence on Twentieth-century precipitation trends. *Nature*, *448*(7152), 461–465. https://doi.org/10.1038/nature06025

Zhao, T., & Dai, A. (2015). The magnitude and causes of global drought changes in the twenty-first century under a low–moderate emissions scenario. *Journal of Climate*, *28*(11), 4490–4512. https://doi.org/10.1175/jcli-d-14-00363.1

Zhao, T., & Dai, A. (2022). CMIP6 model-projected hydroclimatic and drought changes and their causes in the twenty-first century. *Journal of Climate*, *35*(3), 897–921.

Zhou, S., Williams, A. P., Berg, A. M., Cook, B. I., Zhang, Y., Hagemann, S., et al. (2019). Land–atmosphere feedbacks exacerbate concurrent soil drought and atmospheric aridity. *Proceedings of the National Academy of Sciences*, *116*(38), 18848–18853. https://doi.org/10.1073/pnas.1904955116

Zscheischler, J., Westra, S., van den Hurk, B. J. J. M., Seneviratne, S. I., Ward, P. J., Pitman, A., et al. (2018). Future climate risk from compound events. *Nature Climate Change*, *8*(6), 469–477. https://doi.org/10.1038/s41558-018-0156-3

References From the Supporting Information

Boucher, O., Denvil, S., Levavasseur, G., Cozic, A., Caubel, A., Foujols, M. A., et al. (2018). *IPSL IPSL-CM6A-LR model output prepared for CMIP6 CMIP* (Version 20230220) [Application/x-netcdf]. Earth System Grid Federation. https://doi.org/10.22033/ESGF/CMIP6.1534

Danabasoglu, G. (2019). *NCAR CESM2 model output prepared for CMIP6 CMIP historical* (Version 20230220) [Application/x-netcdf]. Earth System Grid Federation. https://doi.org/10.22033/ESGF/CMIP6.7627

Dix, M., Bi, D., Dobrohotoff, P., Fiedler, R., Harman, I., Law, R., et al. (2019). *CSIRO-ARCCSS ACCESS-CM2 model output prepared for CMIP6 CMIP* (Version 20230220) [Application/x-netcdf]. Earth System Grid Federation. https://doi.org/10.22033/ESGF/CMIP6.2281

EC-Earth Consortium (EC-Earth). (2019). *EC-Earth-Consortium EC-Earth3 model output prepared for CMIP6 CMIP historical* (Version 20230220) [Application/x-netcdf]. Earth System Grid Federation. https://doi.org/10.22033/ESGF/CMIP6.4700

He, B., Bao, Q., Wang, X., Zhou, L., Wu, X., Liu, Y., et al. (2019). CAS FGOALS-f3-L model datasets for CMIP6 historical atmospheric model intercomparison project simulation. *Advances in Atmospheric Sciences*, *36*(8), 771–778. https://doi.org/10.1007/s00376-019-9027-8

Krasting, J. P., John, J. G., Blanton, C., McHugh, C., Nikonov, S., Radhakrishnan, A., et al. (2018). *NOAA-GFDL GFDL-ESM4 model output prepared for CMIP6 CMIP historical* (Version 20230220) [Application/x-netcdf]. Earth System Grid Federation. https://doi.org/10.22033/ESGF/CMIP6.8597

Lee, W.-L., Wang, Y.-C., Shiu, C.-J., Tsai, I., Tu, C.-Y., Lan, Y.-Y., et al. (2020). Taiwan Earth system model version 1: Description and evaluation of mean state [preprint] [Dataset]. *Climate and Earth System Modeling*. https://doi.org/10.5194/gmd-2019-377

Li, L., Yu, Y., Tang, Y., Lin, P., Xie, J., Song, M., et al. (2020). The Flexible Global Ocean-Atmosphere-Land System model grid-point version 3 (FGOALS-g3): Description and evaluation. *Journal of Advances in Modeling Earth Systems*, *12*(9), e2019MS002012. https://doi.org/10.1029/2019MS002012

Lovato, T., & Peano, D. (2020). *CMCC CMCC-CM2-SR5 model output prepared for CMIP6 CMIP historical* (Version 20230220) [Application/x-netcdf]. Earth System Grid Federation. https://doi.org/10.22033/ESGF/CMIP6.3825

Lovato, T., Peano, D., & Butenschön, M. (2021). *CMCC CMCC-ESM2 model output prepared for CMIP6 CMIP historical* (Version 20230213) [Application/x-netcdf]. Earth System Grid Federation. https://doi.org/10.22033/ESGF/CMIP6.13195

Roberts, M. (2017). *MOHC HadGEM3-GC31-LL model output prepared for CMIP6 HighResMIP* (Version 20230220) [Application/x-netcdf]. Earth System Grid Federation. https://doi.org/10.22033/ESGF/CMIP6.1901

Shiogama, H., Abe, M., & Tatebe, H. (2019). *MIROC MIROC6 model output prepared for CMIP6 ScenarioMIP* (Version 20230220) [Application/x-netcdf]. Earth System Grid Federation. https://doi.org/10.22033/ESGF/CMIP6.898

Swart, N. C., Cole, J. N., Kharin, V. V., Lazare, M., Scinocca, J. F., Gillett, N. P., et al. (2019). The Canadian Earth System Model version 5 (CanESM5. 0.3). *Geoscientific Model Development*, *12*(11), 4823–4873. https://doi.org/10.5194/gmd-12-4823-2019

Tang, Y., Rumbold, S., Ellis, R., Kelley, D., Mulcahy, J., Sellar, A., et al. (2019). *MOHC UKESM1.0-LL model output prepared for CMIP6 CMIP historical* (Version 20230220) [Application/x-netcdf]. Earth System Grid Federation. https://doi.org/10.22033/ESGF/CMIP6.6113

Volodin, E., Mortikov, E., Gritsun, A., Lykossov, V., Galin, V., Diansky, N., et al. (2019). *INM INM-CM4-8 model output prepared for CMIP6 CMIP piControl* (Version 20230220) [Application/x-netcdf]. Earth System Grid Federation. https://doi.org/10.22033/ESGF/CMIP6.5080

von Storch, J.-S., Putrasahan, D., Lohmann, K., Gutjahr, O., Jungclaus, J., Bittner, M., et al. (2017). *MPI-M MPIESM1.2-HR model output prepared for CMIP6 HighResMIP* (Version 20230220) [Application/x-netcdf]. Earth System Grid Federation. https://doi.org/10.22033/ESGF/CMIP6.762

Wieners, K.-H., Giorgetta, M., Jungclaus, J., Reick, C., Esch, M., Bittner, M., et al. (2019). *MPI-M MPI-ESM1.2-LR model output prepared for CMIP6 CMIP historical* (Version 20230220) [Application/x-netcdf]. Earth System Grid Federation. https://doi.org/10.22033/ESGF/CMIP6.6595

Wu, T., Song, L., Li, W., Wang, Z., Zhang, H., Xin, X., et al. (2014). An overview of BCC climate system model development and application for climate change studies. *Acta Meteorologica Sinica*, *28*(1), 34–56. https://doi.org/10.1007/s13351-014-3041-7

Yukimoto, S., Koshiro, T., Kawai, H., Oshima, N., Yoshida, K., Urakawa, S., et al. (2019). *MRI MRI-ESM2.0 model output prepared for CMIP6 CMIP* (Version 20230220) [Application/x-netcdf]. Earth System Grid Federation. https://doi.org/10.22033/ESGF/CMIP6.621

Zhang, H., Zhang, M., Jin, J., Fei, K., Ji, D., Wu, C., et al. (2020). Description and climate simulation performance of CAS-ESM Version 2. *Journal of Advances in Modeling Earth Systems*, *12*(12), e2020MS002210. https://doi.org/10.1029/2020MS002210

Ziehn, T., Chamberlain, M., Lenton, A., Law, R., Bodman, R., Dix, M., et al. (2019). *CSIRO ACCESS-ESM1.5 model output prepared for CMIP6 CMIP* (Version 20230220) [Application/x-netcdf]. Earth System Grid Federation. https://doi.org/10.22033/ESGF/CMIP6.2288